# Articles

## To Fuse or Not To Fuse? Reactions of $[HM_4(CO)_{12}BH]^-$ (M = Fe, Ru) with (Phosphine)gold(I) Chlorides. Molecular Structures of $HFe_4(CO)_{12}BHAuP(2\text{-}Me\text{-}C_6H_4)_3$, $[Au(PMePh_2)_2][\{HFe_4(CO)_{12}BH\}_2Au]$, and $[PPN][\{HRu_4(CO)_{12}BH\}_2Au]$

Sylvia M. Draper, Catherine E. Housecroft,* Jacqueline E. Rees, and Musa S. Shongwe

*University Chemical Laboratory, Lensfield Road, Cambridge CB2 1EW, U.K.*

Brian S. Haggerty and Arnold L. Rheingold*

*Department of Chemistry, University of Delaware, Newark, Delaware 19716*

*Received December 16, 1991*

The reaction of $[HFe_4(CO)_{12}BH][PPN]$ (PPN = bis(triphenylphosphine)nitrogen(1+)) with 1 equiv of LAuCl (L = $P(2\text{-}Me\text{-}C_6H_4)_3$, $P(c\text{-}C_6H_{11})_3$) yields $HFe_4(CO)_{12}BHAuL$, but of these two products only $HFe_4(CO)_{12}BHAuP(2\text{-}Me\text{-}C_6H_4)_3$ (1) is stable in solution. Attempts to prepare other monogold derivatives with L = $PMe_3$, $PEt_3$, $PMe_2Ph$, $PMePh_2$ led instead to the ionic product $[AuL_2][\{HFe_4(CO)_{12}BH\}_2Au]$ ($[AuL_2][4]$), which possesses the same stoichiometry as the target molecule $HFe_4(CO)_{12}BHAuL$ but is produced as a result of Au-P bond cleavage and a ligand redistribution reaction. The ruthenium cluster $HRu_4(CO)_{12}BHAuP(2\text{-}Me\text{-}C_6H_4)_3$ (2) may be prepared by a corresponding route to that used for 1, but unlike 1, formation of 2 competes not only with formation of $[AuL_2][\{HRu_4(CO)_{12}BH\}_2Au]$ ($[AuL_2][5]$) but also with that of the digold derivative $Ru_4(CO)_{12}BHAu_2\{P(2\text{-}Me\text{-}C_6H_4)_3\}_2$ (3). Both 1 and 2 are readily deprotonated by $NEt_3$ with loss of Fe-H-Fe or Ru-H-B protons, respectively. Treatment of $[HFe_4(CO)_{12}BH][PPN]$ with ClAu(dppm)AuCl (dppm = bis(diphenylphosphino)methane) leads to a mixture of the borido cluster $HFe_4(CO)_{12}Au_2(dppm)B$ (6; 40%) and the salt $[PPN][\{HFe_4(CO)_{12}BH\}_2Au]$ ($[PPN][4]$; 30%), while in the analogous reaction of $[HRu_4(CO)_{12}BH][PPN]$ with ClAu(dppm)AuCl, the predominant cluster product is $[PPN][5]$. The observed results are discussed in terms of (i) the differing sizes of the $Fe_4$ and $Ru_4$ butterfly frameworks and (ii) the steric constraints of the phosphine ligands. The molecular structures of 1, $[Au(PMePh_2)_2][4]$, and $[PPN][5]$ are presented. 1: triclinic, $P\bar{1}$; $a$ = 10.023 (2) Å, $b$ = 12.814 (3) Å, $c$ = 15.231 (4) Å; $\alpha$ = 104.02 (2)°, $\beta$ = 90.47 (2)°, $\gamma$ = 90.13 (2)°; $V$ = 1897.8 (9) Å$^3$; $Z$ = 2; $R(F)$ = 4.41%. $[Au(PMePh_2)_2][4]$: monoclinic, $C2/c$; $a$ = 21.704 (3) Å, $b$ = 9.542 (2) Å, $c$ = 29.717 (6) Å; $\beta$ = 97.50 (1)°; $V$ = 6102.0 (19) Å$^3$; $Z$ = 4; $R(F)$ = 4.59%. $[PPN][5]$: triclinic, $P\bar{1}$; $a$ = 9.759 (4) Å, $b$ = 13.898 (5) Å, $c$ = 26.964 (17) Å; $\alpha$ = 96.68 (4)°, $\beta$ = 97.31 (4)°, $\gamma$ = 91.78 (4)°; $V$ = 3599 (3) Å$^3$; $Z$ = 2; $R(F)$ = 7.65%. The structure of each of the anions $[4]^-$ and $[5]^-$ exhibits two cluster subunits fused together in a "face-to-face" orientation via a single gold atom. In $[4]^-$ the subunits are mutually cis and there is a spiro twist of 30.9 (5)° at the gold atom. However, in $[5]^-$, the cluster subunits are arranged in a trans configuration, as would be expected on the basis of steric arguments.

Recently, we have reported[1-9] some reactions of (phosphine)gold(I) chlorides, LAuCl, with the metallaborane clusters $[HM_4(CO)_{12}BH]^-$ (M = Fe, Ru). The (phosphine)gold(I) products so far reported by us fall into three structural categories: I (monogold derivative, $HM_4(CO)_{12}BHAuL$, M = Fe, Ru),[3,8] II (digold derivative, $HM_4(CO)_{12}BAu_2L_2$, M = Fe, Ru, for which the two isomers IIa and IIb are observed),[1-3,5,7-9] and III (trigold derivative, $Fe_4(CO)_{12}BAu_3L_3$).[4] The replacement of a cluster-bound

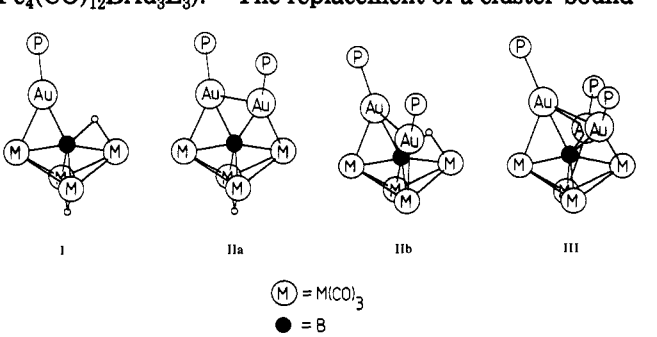


hydrogen atom by a gold(I) phosphine fragment is a common phenomenon in cluster chemistry, and there are many examples in which more than one hydrogen atom has been replaced.[10] In most instances, monogold derivatives ap-

(1) Housecroft, C. E.; Rheingold, A. L. *J. Am. Chem. Soc.* **1986**, *108*, 6420.
(2) Housecroft, C. E.; Rheingold, A. L. *Organometallics* **1987**, *6*, 1332.
(3) Harpp, K. S.; Housecroft, C. E. *J. Organomet. Chem.* **1988**, *340*, 389.
(4) Harpp, K. S.; Housecroft, C. E.; Rheingold, A. L.; Shongwe, M. S. *J. Chem. Soc., Chem. Commun.* **1988**, 965.
(5) Housecroft, C. E.; Rheingold, A. L.; Shongwe, M. S. *Organometallics* **1988**, *7*, 1885.
(6) Housecroft, C. E.; Rheingold, A. L.; Shongwe, M. S. *J. Chem. Soc., Chem. Commun.* **1988**, 1630.
(7) Housecroft, C. E.; Rheingold, A. L.; Shongwe, M. S. *Organometallics* **1989**, *8*, 2651.
(8) Chipperfield, A. K.; Housecroft, C. E.; Rheingold, A. L. *Organometallics* **1990**, *9*, 681.
(9) Housecroft, C. E.; Shongwe, M. S.; Rheingold, A. L.; Zanello, P. *J. Organomet. Chem.* **1991**, *408*, 7.
(10) Salter, I. M. *Adv. Organomet. Chem.* **1989**, *29*, 249.

0276-7333/92/2311-2356$03.00/0 

pear to form easily and are stable products. However, in a preliminary communication we reported that the reaction of LAuCl with $[HFe_4(CO)_{12}BH][PPN]$, in the presence of $TlPF_6$ for L = $PMe_3$, $PEt_3$, $PMe_2Ph$, $PMePh_2$, leads to Au–P bond cleavage and gives the ionic product $[AuL_2][\{HFe_4(CO)_{12}BH\}_2Au]$ instead of the stoichiometrically equivalent compound $HFe_4(CO)_{12}BHAuL$.[6] The fusion of two cluster fragments about a gold(I) atom is still an infrequent observation, as is fusion about Ag(I) or Cu(I) centers.[10] We now report in full an investigation of the stoichiometrically controlled reactions of $[HFe_4(CO)_{12}BH][PPN]$ with LAuCl (L = P(2-Me-$C_6H_4$)$_3$, P($c$-$C_6H_{11}$)$_3$), $PMe_3$, $PEt_3$, $PMe_2Ph$, $PMePh_2$) and include a comparison of the reactions of $[HFe_4(CO)_{12}BH][PPN]$ and $[HRu_4(CO)_{12}BH][PPN]$ with (2-Me-$C_6H_4$)$_3$PAuCl and ClAu(dppm)AuCl.

## Experimental Section

**General Data.** FT-NMR spectra were recorded on a Bruker WM 250 or AM 400 spectrometer. $^1H$ NMR shifts are reported with respect to $\delta$ 0 for $Me_4Si$, $^{11}B$ NMR shifts with respect to $\delta$ 0 for $F_3B{\cdot}OEt_2$, and $^{31}P$ NMR shifts with respect to $\delta$ 0 for $H_3PO_4$. All downfield chemical shifts are positive. Infrared spectra were recorded on a Perkin-Elmer FT 1710 spectrophotometer. FAB mass spectra were recorded on a Kratos MS 50TC, MS 902, or MS 890 instrument.

All reactions were carried out under argon by using standard Schlenk techniques. Solvents were dried over suitable reagents and freshly distilled under $N_2$ before use. Separations were carried out either by centrifugal chromatography (iron clusters) with Kieselgel 60-PF-254 mesh (Merck) or by thin-layer plate chromatography (ruthenium clusters) with Kieselgel 60-PF-254 (Merck). (Phosphine)gold(I) chlorides were prepared from $HAuCl_4{\cdot}3H_2O$ (Aldrich) and $PMe_2Ph$, $PEt_3$, and dppm (bis(diphenylphosphino)methane Aldrich) and P(2-Me-$C_6H_4$)$_3$, P($c$-$C_6H_{11}$)$_3$), $PMe_3$, and $PMePh_2$ (Strem) by methods based on those reported in the literature.[11,12] $[PPN][HFe_4(CO)_{12}BH]$[13] and $[PPN][HRu_4(CO)_{12}BH]$[8] were prepared as previously reported.

**Preparation of $HFe_4(CO)_{12}BHAu\{P(2\text{-}Me\text{-}C_6H_4)_3\}$ (1).** $CH_2Cl_2$ (20 mL) was added to a mixture of solid $[PPN][HFe_4(CO)_{12}BH]$ (0.15 g, 0.14 mmol), $\{(2\text{-}Me\text{-}C_6H_4)_3\}PAuCl$ (0.07 g, 0.13 mmol), and $TlPF_6$ (0.05 g, 0.28 mmol). When the mixture was stirred, the color changed immediately from red-brown to dark green. After 45 min, $Et_2O$ (10 mL) was added to precipitate $[PPN][PF_6]$ and TlCl. The mixture was filtered, the filtrate collected, and the solvent removed. Products were separated chromatographically by eluting with $CH_2Cl_2$–hexane (1:1), and 1 was collected as the first (light green) fraction in ~80% yield (0.12 g, 0.11 mmol): 250-MHz $^1H$ NMR ($CD_2Cl_2$) $\delta$ 7.6–6.9 (m, *Ph*), 2.65 (s, *Me*), –7.7 (br, Fe–*H*–B), –24.9 (s, Fe–*H*–Fe); 128-MHz $^{11}B$ NMR ($CD_2Cl_2$) $\delta$ +136.0; 162-MHz $^{31}P$ NMR ($CD_2Cl_2$) $\delta$ +45; IR ($CH_2Cl_2$, $cm^{-1}$) $\nu_{CO}$ 2076 w, 2031 vs, 2028 vs, 2009 m, 1990 m; FAB-MS in 3-NBA matrix $m/z$ 1074 ($P^+$), isotopic pattern is consistent with that simulated.

**Deprotonation of 1.** Neat $Et_3N$ (0.30 mL) was added to 1 (0.08 g, 0.07 mmol) which was previously dissolved in $CH_2Cl_2$ (5 mL). The solution was placed in an ultrasonic bath for 10 min, during which time the color changed from light green to green-brown. Solvent was removed, and the product was washed with hexane (4 × 10 mL). The solid product (approximately quantitative yield) was dried under reduced pressure. $[Et_3NH][Fe_4(CO)_{12}BHAuP\{(2\text{-}Me\text{-}C_6H_4)_3\}]$: 250-MHz $^1H$ NMR ($CD_2Cl_2$) $\delta$ 7.6–6.9 (m, *Ph*), 3.44 (q, $J_{HH}$ = 7 Hz, $CH_2$(*Et*)), 2.67 (s, *Me*), 1.16 (t, $J_{HH}$ = 7 Hz, $CH_3$(*Et*)), –9.4 (br, Fe–*H*–B); 128-MHz $^{11}B$ NMR ($CD_2Cl_2$) $\delta$ +137.0; 162-MHz $^{31}P$ NMR ($CD_2Cl_2$) $\delta$ +45; IR ($CH_2Cl_2$, $cm^{-1}$) $\nu_{CO}$ 2026 m, 2024 sh, 1992 s, 1989 sh, 1962 m; FAB-MS in 3-NBA matrix $m/z$ 1073 ($P^-$) with 12 CO loss observed, isotopic pattern is consistent with that simulated.

**Preparation of $HFe_4(CO)_{12}BHAu\{P(c\text{-}C_6H_{11})_3\}$.** The methods of synthesis and separation were the same as for 1 but with $[PPN][HFe_4(CO)_{12}BH]$ (0.25 g, 0.23 mmol), $\{(c\text{-}C_6H_{11})_3\}PAuCl$ (0.10 g, 0.23 mmol), and $TlPF_6$ (0.16 g, 0.46 mmol). $HFe_4(CO)_{12}BHAu\{P(c\text{-}C_6H_{11})_3\}$ was isolated as a light green solid in ~90% yield (0.22 g, 0.21 mmol): 250-MHz $^1H$ NMR ($CD_2Cl_2$) $\delta$ 1.4–2.2 (m, $CH_2$), –7.3 (br, Fe–*H*–B), –24.9 (s, Fe–*H*–Fe); 128-MHz $^{11}B$ NMR ($CD_2Cl_2$) $\delta$ +139.0; 162-MHz $^{31}P$ NMR ($CD_2Cl_2$) $\delta$ +70; IR ($CH_2Cl_2$, $cm^{-1}$) $\nu_{CO}$ 2076 w, 2030 vs, 2028 vs, 2007 m, 1990 m; FAB-MS in 3-NBA matrix $m/z$ 1050 ($P^+$) isotopic pattern is consistent with that simulated.

**Preparation of $[Au\{P(2\text{-}Me\text{-}C_6H_4)_3\}_2][\{HFe_4(CO)_{12}BH\}_2Au]$ ($[Au\{P(2\text{-}Me\text{-}C_6H_4)_3\}_2][4]$).** $CH_2Cl_2$ (15 mL) was added to solid $[PPN][HFe_4(CO)_{12}BH]$ (0.23 g, 0.21 mmol), excess $\{(2\text{-}Me\text{-}C_6H_4)_3\}PAuCl$ (0.33 g, 0.62 mmol), and $TlPF_6$ (0.22 g, 0.63 mmol). When the mixture was stirred, the color changed immediately from red-brown to dark green-brown. After 45 min, $Et_2O$ (10 mL) was added. The mixture was filtered, the filtrate collected, and the solvent removed. Products were separated chromatographically by eluting with $CH_2Cl_2$–hexane (1:1), and $[Au\{P(2\text{-}Me\text{-}C_6H_4)_3\}_2][4]$ was collected as the second (dark green) fraction in ~50% yield (0.11 g, 0.05 mmol). The first fraction (30% yield) was 1. $[4]^-$: 250-MHz $^1H$ NMR ($CD_2Cl_2$) $\delta$ –6.4 (br, Fe–*H*–B), –24.9 (s, Fe–*H*–Fe); 128-MHz $^{11}B$ NMR ($CD_2Cl_2$) $\delta$ +134.0; IR ($CH_2Cl_2$, $cm^{-1}$) $\nu_{CO}$ 2065 w, 2033 vs, 2002 m, 1980 m; FAB-MS in 3-NBA matrix $m/z$ 1343 ($P^-$), isotopic pattern is consistent with that simulated. The $[Au\{P2\text{-}Me\text{-}C_6H_4)_3\}_2]^+$ cation was characterized by 162-MHz $^{31}P$ NMR ($CD_2Cl_2$): $\delta$ +15.

**Preparation of $[AuL_2][4]$, L = $PMe_3$, $PEt_3$, $PMe_2Ph$, $PMePh_2$.** These compounds were obtained in yields of 5–15% as byproducts in the previously described preparations of the digold derivatives $HFe_4(CO)_{12}BAu_2L_2$.[7] The latter remained the predominant products even when the ratio of $[HFe_4(CO)_{12}BH][PPN]$ to LAuCl was 1:1. Spectroscopic characteristics of the anion $[\{HFe_4(CO)_{12}BH\}_2Au]^-$ were as given for $[4]^-$ in $[Au\{P(2\text{-}Me\text{-}C_6H_4)_3\}_2][4]$ and were independent of the cation. $^{31}P$ NMR resonances for the $[AuL_2]^+$ cations were in agreement with literature values.[14]

**Reaction of $[HFe_4(CO)_{12}BH][PPN]$ with ClAu(dppm)AuCl.** $CH_2Cl_2$ (10 mL) was added to $[PPN][HFe_4(CO)_{12}BH]$ (0.41 g, 0.37 mmol), ClAu(dppm)AuCl (0.31 g, 0.37 mmol), and $TlPF_6$ (0.02 g, 0.06 mmol). After the mixture was stirred, a color change from red-brown to yellow-brown was observed. After 45 min the solvent was removed in vacuo. The products were extracted with $Et_2O$ (4 × 10 mL) and then separated chromatographically by eluting with hexane followed by $CH_2Cl_2$. The first (dark green) band to be eluted was identified from its IR spectrum as $Fe_3(CO)_{12}$. The second (brown) band was $HFe_4(CO)_{12}Au_2$(dppm)B (6; ~40%, 0.20 g, 0.15 mmol), and the third (lime green) fraction was characterized as $[PPN][4]$ (~30%, 0.11 g, 0.06 mmol). A fourth product, which was red-brown and contained boron, was not fully characterized. 6: 250-MHz $^1H$ NMR ($CD_2Cl_2$, 298 K) $\delta$ 7.6–7.3 (m, *Ph*), 3.4 (t, $J_{PH}$ = 7 Hz, $CH_2$), –23.9 (s, Fe–*H*–Fe); 128-MHz $^{11}B$ NMR ($CD_2Cl_2$) $\delta$ +184.5; 162-MHz $^{31}P$ NMR ($CD_2Cl_2$) $\delta$ +43.8; IR ($CH_2Cl_2$, $cm^{-1}$) $\nu_{CO}$ 2058 m, 2030 sh, 2017 vs, 2008 s, 1978 m, 1930 w; FAB-MS in 3-NBA matrix $m/z$ 1350 ($P^+$), isotopic pattern is consistent with that simulated.

**Preparation of $HRu_4(CO)_{12}BHAu\{P(2\text{-}Me\text{-}C_6H_4)_3\}$ (2) and $Ru_4(CO)_{12}BHAu_2\{P(2\text{-}Me\text{-}C_6H_4)_3\}_2$ (3).** $CH_2Cl_2$ (10 mL) was added to solid $[PPN][HRu_4(CO)_{12}BH]$ (0.26 g, 0.20 mmol), (2-Me-$C_6H_4$)$_3$PAuCl (0.08 g, 0.15 mmol), and $TlPF_6$ (0.02 g, 0.06 mmol), and the resulting solution was stirred for 15 min. A color change from orange to dark brown was observed. The products were separated by TLC and were eluted with $CH_2Cl_2$–hexane (1:1). The first (yellow) band to be eluted was $H_4Ru_4(CO)_{12}$. The second (yellow) band was $[Au\{P(2\text{-}Me\text{-}C_6H_4)_3\}_2][5]$ (yield ~5%; see below). The two major products were $HRu_4(CO)_{12}BHAu\{P(2\text{-}Me\text{-}C_6H_4)_3\}$ (2) and $Ru_4(CO)_{12}BHAu_2\{P(2\text{-}Me\text{-}C_6H_4)_3\}_2$ (3) and were separated as the third (dark orange, yield ~15%, 0.04 g, 0.03 mmol) and fourth (bright orange, yield ~30%, 0.11 g, 0.06 mmol) bands, respectively. 2: 250-MHz $^1H$ NMR ($CD_2Cl_2$, 298 K) $\delta$ 7.6–7.2 (m, *Ph*), 2.7 (s, *Me*), –4.7 (br, Ru–*H*–B), –20.8 (s, Ru–*H*–Ru); 128-MHz $^{11}B$ NMR ($CD_2Cl_2$) $\delta$ +132.1; 162-MHz $^{31}P$ NMR

(11) Mann, F. G.; Wells, A. F.; Purdie, D. *J. Chem. Soc.* **1937**, 1823.
(12) Williamson, D. R.; Baird, M. C. *J. Inorg. Nucl. Chem.* **1972**, *34*, 3393.
(13) Housecroft, C. E.; Buhl, M. L.; Long, G. J.; Fehlner, T. P. *J. Am. Chem. Soc.* **1987**, *109*, 3323.
(14) Parish, R. V.; Parry, O.; McAuliffe, C. A. *J. Chem. Soc., Dalton Trans.* **1981**, 2098 and references therein.

**Table I. Crystal Data for Compounds 1, [Au(PMePh$_2$)$_2$][4], and [PPN][5]**

| | 1 | [Au(PMePh$_2$)$_2$][4] | [PPN][5] |
|---|---|---|---|
| | (a) Crystal Parameters | | |
| formula | $C_{33}H_{23}AuBFe_4O_{12}P$ | $C_{50}H_{30}Au_2B_2Fe_8O_{24}P_2$ | $C_{60}H_{34}AuB_2NO_{24}P_2Ru_8$ |
| fw | 1073.68 | 1939.05 | 2242.02 |
| cryst syst | triclinic | monoclinic | triclinic |
| space group | $P\bar{1}$ | $C2/c$ | $P\bar{1}$ |
| $a$, Å | 10.023 (2) | 21.704 (3) | 9.759 (4) |
| $b$, Å | 12.814 (3) | 9.542 (2) | 13.898 (5) |
| $c$, Å | 15.231 (4) | 29.717 (6) | 26.964 (17) |
| $\alpha$, deg | 104.02 (2) | | 96.68 (4) |
| $\beta$, deg | 90.47 (2) | 97.50 (1) | 97.31 (4) |
| $\gamma$, deg | 90.13 (2) | | 91.78 (3) |
| $V$, Å$^3$ | 1897.8 (9) | 6102.0 (19) | 3599 (3) |
| $Z$ | 2 | 4 | 2 |
| cryst dimens, mm | 0.22 × 0.27 × 0.32 | 0.20 × 0.20 × 0.40 | 0.18 × 0.32 × 0.40 |
| cryst color | dark brown | dark orange | light brown |
| $D$(calc), g cm$^{-3}$ | 1.879 | 2.111 | 2.069 |
| $\mu$(Mo K$\alpha$), cm$^{-1}$ | 54.37 | 69.7 | 29.5 |
| temp, K | 293 | 293 | 293 |
| $T$(max)/$T$(min) | 1.72 | 1.63 | 2.20 |
| | (b) Data Collection | | |
| diffractometer | | Nicolet R3M | |
| monochromator | | graphite | |
| radiation | | Mo K$\alpha$ ($\lambda$ = 0.71073 Å) | |
| 2$\theta$ scan range, deg | 4–50 | 4–48 | 4–45 |
| data collected | $\pm h,\pm k,+l$ | $\pm h,k,l$ | $\pm h,\pm k,+l$ |
| no. of rflns collected | 6948 | 5220 | 9587 |
| no. of indpt rflns | 6520 | 4785 | 9354 |
| no. of indpt obs rflns, $F_o \geq 4\sigma(F_o)$ | 5155 | 3050 | 6954 |
| std rflns | | 3 stds/197 rflns | |
| var in stds, % | ~2 | ~5 | ~5 |
| | (c) Refinement | | |
| $R(F)$, % | 4.41 | 4.59 | 7.65 |
| $R$(w$F$), % | 4.72 | 6.22 | 7.70 |
| $\Delta/\sigma$(max) | 0.22 | 0.13 | 0.08 |
| $\Delta(\rho)$, e Å$^{-3}$ | 1.29 | 1.02 | 4.07 |
| $N_o/N_v$ | 10.99 | 8.65 | 10.97 |
| GOF | 1.341 | 1.032 | 1.644 |

($CD_2Cl_2$) $\delta$ +57.4; IR ($CH_2Cl_2$, cm$^{-1}$) $\nu_{CO}$ 2089 m, 2064 m sh, 2051 vs, 2034 s, 2012 m, 2000 w, 1983 m, 1969 w, 1959 w; FAB-MS in 3-NBA matrix $m/z$ 1248 ($P^+$) isotopic pattern is consistent with that simulated. **3**: 250-MHz $^1$H NMR ($CD_2Cl_2$, 298 K) $\delta$ 7.7–7.1 (m, *Ph*), 2.7 (s, *Me*), −4.7 (br, Ru-*H*-B); 128-MHz $^{11}$B NMR ($CD_2Cl_2$) $\delta$ +132.2; 162-MHz $^{31}$P NMR ($CD_2Cl_2$) $\delta$ +63.8, +37.3 (see text); IR ($CH_2Cl_2$, cm$^{-1}$) $\nu_{CO}$ 2068 w, 2039 vs, 2019 s, 1998 m, 1985 m, 1961 w; FAB-MS in 3-NBA matrix $m/z$ 1754 ($P^+$), isotopic pattern is consistent with that simulated.

**Deprotonation of 2.** Neat $Et_3N$ (0.15 mL) was added to **2** (0.03 g, 0.02 mmol) which was previously dissolved in $CH_2Cl_2$ (0.7 mL). The solution changed from red-orange to dark brown. Solvent was removed and the product washed with hexane (5 × 5 mL). [$Et_3NH$][$HRu_4(CO)_{12}BAuP\{(2\text{-Me-}C_6H_4)_3\}$]: 250-MHz $^1$H NMR ($CD_2Cl_2$) $\delta$ 7.6–7.1 (m, *Ph*), 3.42 (q, $J_{HH}$ = 7 Hz, $CH_2(Et)$), 2.68 (s, *Me*), 1.45 (t, $J_{HH}$ = 7 Hz, $CH_3(Et)$), −20.9 (s, Ru-*H*-Ru); 128-MHz $^{11}$B NMR ($CD_2Cl_2$) $\delta$ +171.4; 162-MHz $^{31}$P NMR ($CD_2Cl_2$) $\delta$ +57.5; IR ($CH_2Cl_2$, cm$^{-1}$) $\nu_{CO}$ 2086 w, 2050 s, 2040 m sh, 2018 s, 1999 s; FAB-MS in 3-NBA matrix $m/z$ 1252 ($P^-$) with 5 CO loss observed, isotopic pattern is consistent with that simulated.

**Preparation of [PPN][{$HRu_4(CO)_{12}BH$}$_2$Au] ([PPN][5]).** The anion [**5**]$^-$ may be prepared as its [PPN]$^+$ salt via the reaction of [PPN][$HRu_4(CO)_{12}BH$] with ClAu(dppm)AuCl.[15] $CH_2Cl_2$ (10 mL) was added to [PPN][$HRu_4(CO)_{12}BH$] (0.13 g, 0.10 mmol), ClAu(dppm)AuCl (0.09 g, 0.10 mmol), and $TlPF_6$ (0.02 g, 0.06 mmol). The solution was stirred for 45 min, during which time the color changed from yellow-orange to dark brown. After extraction with $Et_2O$, the products were separated chromatographically by eluting with $CH_2Cl_2$–hexane (1:1). [PPN][**5**] was collected as the fourth (bright yellow) fraction (~40%, 0.04 g, 0.02 mmol) and was the only major product. Several other minor products were not collected. [**5**]$^-$: 250-MHz $^1$H NMR ($CD_2Cl_2$) $\delta$ −4.1 (br, Ru-*H*-B), −20.9 (s, Ru-*H*-Ru); 128-MHz $^{11}$B NMR ($CD_2Cl_2$) $\delta$ +133.9; IR ($CH_2Cl_2$, cm$^{-1}$) $\nu_{CO}$ 2077 s, 2050 vs, 2024 w, 1992 m; FAB-MS in 3-NBA matrix $m/z$ 1706 ($P^-$), isotopic pattern is consistent with that simulated. The [PPN]$^+$ cation was characterized: 162-MHz $^{31}$P NMR ($CD_2Cl_2$) $\delta$ +21.1; 250-MHz $^1$H NMR ($CD_2Cl_2$) $\delta$ 7.6–7.3 (m).

**Crystal Structure Determinations. General Data.** Suitable crystals of **1** and [PPN][**5**] were grown from $CH_2Cl_2$ solutions layered with hexane. X-ray-quality crystals of [Au{$PMePh_2$}$_2$][**4**] were obtained by using a fortuitous mix of $PMePh_2$ and $PMe_2Ph$ (~2:1) and were grown from a $CH_2Cl_2$ solution layered with hexane. All specimens were mounted on glass fibers and were initially characterized photographically. Crystals of **1** and [PPN][**5**] revealed only triclinic symmetry, and [Au{$PMePh_2$}$_2$][**4**] showed monoclinic symmetry. In all cases the centrosymmetric alternative space group was perferred on the basis of the chemically reasonable results of refinement. All of the structures were corrected for absorption by empirical procedures. They were all solved by auto-interpreted Patterson maps. In the structures of [Au{$PMePh_2$}$_2$][**4**] and [PPN][**5**], the phenyl rings were rigidly constrained. For [PPN][**5**], the asymmetric unit consists of the halves of the anion and a whole PPN counterion. The Au atom in [Au{$PMePh_2$}$_2$][**4**] was disordered over two chemically equivalent sites, labeled Au(1) at 80.2 (1)% occupancy and Au(3) at 19.8 (1)%. These atoms are on the crystallographic 2-fold axis.

All non-hydrogen atoms were refined with anisotropic thermal parameters, and the hydrogen atoms were idealized except for those bonded to B, Fe, or Ru atoms, which were ignored. All computations and sources of scattering factors used the various components of the SHELXTL (version 5.1) software written by G. Sheldrick for the Nicolet (Siemens) Corp., Madison, WI. Atomic coordinates for **1**, [Au{$PMePh_2$}$_2$][**4**], and [PPN][**5**] are listed in Tables II, V, and VII, respectively.

(15) The anion [**5**]$^-$ has also been obtained as a byproduct in the reaction of [$HRu_4(CO)_{12}BH$]$^-$ with ClAu(L-L)AuCl in which L-L = various bidentate phosphine ligands. Draper, S. M. Ph.D. Thesis, University of Cambridge, 1991.

## Results and Discussion

**Formation of Monogold Derivatives $HM_4(CO)_{12}BHAuL$ (M = Fe, L = P(*c*-$C_6H_{11})_3$, P(2-Me-$C_6H_4)_3$; M = Ru, L = P(2-Me-$C_6H_4)_3$).** In an earlier paper,[7] we described the syntheses of and structural variations exhibited by digold clusters of type $HFe_4(CO)_{12}BAu_2L_2$ (structure IIa or IIb) in which L is a monodentate phosphine ligand with a Tolman cone angle ($\theta$)[16,17] in the range $118° \leq \theta \leq 170°$. This corresponds to phosphine ligands ranging in size from $PMe_3$ to P(*c*-$C_6H_{11})_3$. We also stated[7] that attempts to make a related compound for L = P(2-Me-$C_6H_4)_3$ ($\theta$ = 194°) had failed.

The reaction of $[HFe_4(CO)_{12}BH]^-$ with (2-Me-$C_6H_4)_3$PAuCl proceeds by the simple addition of one gold(I) phosphine fragment to the cluster to generate $HFe_4(CO)_{12}BHAuP(2\text{-Me-}C_6H_4)_3$ (1). Interestingly, 1 is the only stable monogold derivative of the tetrairon butterfly cluster that we have been able to isolate,[18] and we attribute this particular stability to the steric requirements of the tris(*o*-tolyl)phosphine ligand. In general the digold derivative II is preferred over a type I product.[7] This phenomenon is observed even with the relatively bulky tris(cyclohexyl)phosphine ligand ($\theta$ = 170°). The reaction of equimolar quantities of $[HFe_4(CO)_{12}BH]^-$ with (*c*-$C_6H_{11})_3$PAuCl gives $HFe_4(CO)_{12}BHAuP(c\text{-}C_6H_{11})_3$ in ~90% yield, but when a dichloromethane solution of this cluster is left to stand, slow conversion to $Fe_4(CO)_{12}BHAu_2\{P(c\text{-}C_6H_{11})_3\}_2$ occurs, with almost complete conversion being observed within 5–7 days. Attempts to crystallize $HFe_4(CO)_{12}BHAuP(c\text{-}C_6H_{11})_3$ from $CH_2Cl_2$–hexane mixtures resulted in the formation of crystals of $Fe_4(CO)_{12}BHAu_2\{P(c\text{-}C_6H_{11})_3\}_2$. In the presence of methanol, the monogold → digold conversion occurred more rapidly. The size of the phosphine ligand is clearly the critical factor; for example, methanol–dichloromethane–hexane solutions of $HFe_4(CO)_{12}BHAuPPh_3$[3] left to stand yielded crystals of $Fe_4(CO)_{12}BAu_3(PPh_3)_3$ (structure III).[4] Crystallographic data are available for a range of $Fe_4B$-based gold(I) phosphine derivatives, and the parameters illustrate that the butterfly framework resists geometrical change when cluster-bound hydrogen atoms are replaced by the much larger gold(I) phosphine electrophiles.[19] From the present study, it is concluded that the steric requirements of two AuP(2-Me-$C_6H_4)_3$ groups ($\theta_{phosphine}$ = 194°) plus one hydrogen atom are greater than the demands of three $AuPPh_3$ fragments ($\theta_{phosphine}$ = 145°). In addition, we note that the $\{Fe_4(CO)_{12}B\}$ cluster framework is too small to accommodate more than one AuP(2-Me-$C_6H_4)_3$ fragment.

The transition from $HFe_4(CO)_{12}BH_2$ to $HRu_4(CO)_{12}BH_2$ is accompanied by a significant increase in the size the $M_4B$ framework. This manifests itself in a change of structure for the derivatives $HM_4(CO)_{12}BAu_2\{PPh_3\}_2$ in going from M = Fe to M = Ru.[1,2,8] Since we had found compound 1 (cluster type I) to be stable with respect to conversion to higher nuclearity derivatives of types II and III, it was of interest to examine whether the corresponding auraruthenaborane would also be stable or whether the larger tetrametal framework would permit the formation of clusters of type II or even III.

The reaction of $[HRu_4(CO)_{12}BH]^-$ with (2-Me-$C_6H_4)_3$PAuCl in the presence of $TlPF_6$ leads to three isolable boron-containing products, identified as $HRu_4(CO)_{12}BHAuP(2\text{-Me-}C_6H_4)_3$ (2; ~15% yield), $HRu_4(CO)_{12}BAu_2\{P(2\text{-Me-}C_6H_4)_3\}_2$ (3; ~30% yield), and [PPN][$\{HRu_4(CO)_{12}BH\}_2Au$] ([PPN][5]; ~5% yield). A fourth product was observed in the crude mixture, but it could not be isolated. This is proposed to be $Ru_4(CO)_{12}BAu_3\{P(2\text{-Me-}C_6H_4)_3\}_3$; the $^{11}B$ NMR spectrum has a signal at $\delta$ +172, and in the $^1H$ NMR spectrum there are no high-field signals additional to those assigned to compounds 2, 3, and $[5]^-$.

The spectroscopic characteristics of 2 allow us to formulate a structure analogous to that of 1. Compound 2 exhibits two high-field proton resonances at $\delta$ −4.7 and −20.8, which are assigned to Ru–H–B and Ru–H–Ru bridging hydrogen atoms, respectively. The $^{11}B$ NMR resonance for 2 at $\delta$ +132.1 is close to that ($\delta$ +137.2) previously reported for $HRu_4(CO)_{12}BHAuPPh_3$.[8] As anticipated, the tetraruthenium butterfly skeleton is sufficiently large to accommodate two AuP(2-Me-$C_6H_4)_3$ groups and the formation of 3 competes significantly with that of 2.

Compound 3 exhibits an $^{11}B$ NMR signal at $\delta$ +132.2, and in the $^1H$ NMR spectrum at 298 K, a single broad resonance at $\delta$ −4.7 is observed. At 190 K, this resonance sharpens due to thermal decoupling of the $^{11}B$–$^1H$ spins but the shift is essentially unaltered ($\delta$ −4.6). These data are not consistent with a structure of type IIa, as crystallographically confirmed for $HRu_4(CO)_{12}BAu_2\{PPh_3\}_2$,[8] but are consistent with an isomer of type IIb in which the steric requirements of the two gold(I) phosphine groups have forced the groups apart with concomitant rearrangement of the hydride and carbonyl ligands in the $\{HRu_4(CO)_{12}B\}$ fragment as seen for related iron systems.[7] Thus, 3 is more correctly formulated as $Ru_4(CO)_{12}\underline{BH}Au_2\{P(2\text{-Me-}C_6H_4)_3\}_2$. Significantly, when reporting details of the triphenylphosphine derivative $HRu_4(CO)_{12}BAu_2\{PPh_3\}_2$, we noted that the structure deviated slightly from $C_2$ symmetry and appeared to lie partway along a path which converted the $M_4Au_2B$ core from its form in isomer IIa to that in IIb.[8] The change from $PPh_3$ (Tolman cone angle $\theta$ = 145°) to P(2-Me-$C_6H_4)_3$ ($\theta$ = 194°) perturbs the system further.[16,17]

Although, taken alone, the $^{11}B$ and $^1H$ NMR spectroscopic data for 3 suggest a structure of type IIb, the $^{31}P$ NMR spectrum of 3 is not as simple as expected. At 298 K, the spectrum exhibits two signals at $\delta$ +63.8 and +37.3, which are of approximately equal intensities. Both resonances are present in redissolved samples of recrystallized 3. As the temperature is lowered to 190 K, the lower field resonance remains sharp but the signal at $\delta$ +37.3 collapses and becomes broad. The observed behavior may be interpreted in terms of the presence of two independent isomers of 3. The chemical shift at $\delta$ +63.8 is in the region expected for the two gold(I) phosphine units bridging an Ru–B edge (compare $\delta$ +57.4 in 2), and we assign this resonance to an isomer with structure IIb. The temperature-independent nature of this $^{31}P$ NMR signal is consistent with a facile process[3,7] that exchanges the two $\{AuP(2\text{-Me-}C_6H_4)_3\}$ groups. The chemical shift of $\delta$ +37.3 is at significantly higher field than would be expected for a phosphorus atom in the environment Ru–Au{P(2-Me-$C_6H_4)_3$}–B but is however consistent with the average of two signals, one corresponding to this environment and one assigned to a Ru–Au{P(2-Me-$C_6H_4)_3$}–Ru bridge. By comparison with published data for the related systems $Ru_4(CO)_{12}CAu_2\{PR_3\}_2$ (see below),[20] we would expect to observe

(16) Tolman, C. A. *J. Am. Chem. Soc.* **1970**, *92*, 2956.
(17) Tolman, C. A. *Chem. Rev.* **1977**, *77*, 313.
(18) We would expect other derivatives of type $HFe_4(CO)_{12}BHAuL$ to be stable if the Tolman cone angle of L is ≥194°: for example, (2,4,6-$Me_3C_6H_2)_3$P, in which $\theta$ = 212°.[17]
(19) Housecroft, C. E. *Adv. Organomet. Chem.* **1991**, *33*, 1.
(20) Cowie, A. G.; Johnson, B. F. G.; Lewis, J.; Raithby, P. R. *J. Chem. Soc., Chem. Commun.* **1984**, 1710.

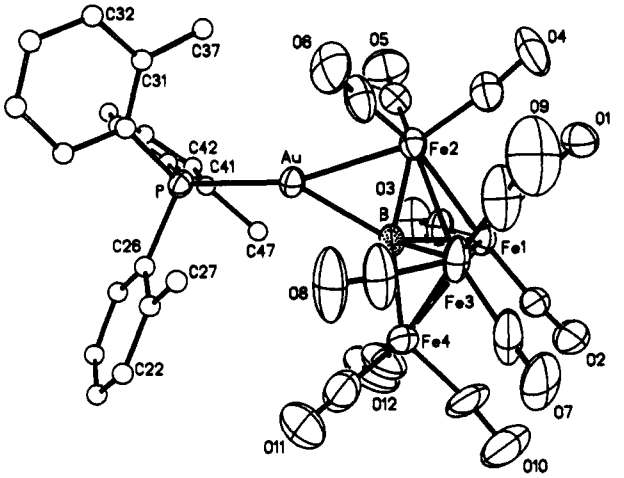


**Figure 1.** Molecular structure and atom numbering of **1**. Hydrogen atoms were not located.

a $^{31}P$ NMR spectral resonance for a butterfly hinge bridging Ru–Au{P(2-Me-$C_6H_4$)$_3$}–Ru unit at a shift similar to that of ClAuP(2-Me-$C_6H_4$)$_3$, viz. $\delta$ +6. An Ru–Ru hinge bridging mode for the $AuPPh_3$ group in $Ru_3Fe(CO)_{12}NAuPPh_3$ has been confirmed crystallographically, and spectroscopic data imply that the $AuPPh_3$ group in $Ru_4(CO)_{12}NAuPPh_3$ is similarly sited.[21] We therefore assign the second $^{31}P$ NMR signal to a second isomer of **3** which has the structure IIc. At 298 K, the Ru–Ru and

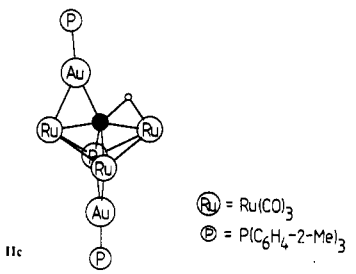


IIc

Ru–B bridging gold(I) phosphine substituents are undergoing exchange on the NMR time scale. The $^{31}P$ NMR spectroscopic data indicate that this exchange process has a higher activation barrier than that in the isomer of **3** with structure IIb.

We would not expect the $^{11}B$ and $^{1}H$ NMR spectroscopic data for the two isomers of **3** to be significantly different from one another; the environment of the boron atom in an isomer with structure IIc is essentially the same as that in **2**. We observe that the $^{11}B$ and $^{1}H$ (for the Ru–H–B bound proton) NMR spectral signatures of **2** and **3** are in fact the same; note that the line widths of the $^{11}B$ NMR signals for **2** and **3** are broad (fwhm = 160 ± 10 Hz).

The proposed structure IIc may be compared to that crystallographically determined for the related butterfly carbide cluster $Ru_4(CO)_{12}CAu_2\{PMe_2Ph\}_2$. Here, one gold(I) phosphine unit bridges the hinge Ru–Ru edge while the second unit bridges completely across the wingtips of the butterfly.[20] Spectroscopic data are consistent with the same structure of $Ru_4(CO)_{12}CAu_2\{PPh_3\}_2$.[20] Formal substitution of the interstitial carbon atom for an isoelectronic {B + H} combination carries with it greater steric requirements. The isomer of **3** with structure IIc is related to that of these carbide clusters, but the presence of the cluster-bound hydrogen atom apparently prevents the formation of the complete Ru(wing)–Au–Ru(wing) bridge.

(21) Blohm, M. L.; Gladfelter, W. L. *Inorg. Chem.* **1987**, *26*, 459.

**Table II. Atomic Coordinates (×10$^4$) and Isotropic Thermal Parameters (Å$^2$ × 10$^3$) for 1**

| | *x* | *y* | *z* | *U*[a] |
|---|---|---|---|---|
| Au | 1943.5 (3) | 2147.3 (3) | 2096.2 (2) | 45.2 (1) |
| Fe(1) | 1927 (1) | 1114 (1) | 4417.9 (8) | 48.4 (4) |
| Fe(2) | 2940 (1) | 635 (1) | 2745.7 (8) | 48.3 (4) |
| Fe(3) | 4273 (1) | 1854 (1) | 4155 (1) | 69.2 (6) |
| Fe(4) | 2267 (2) | 3219 (1) | 4669.1 (9) | 72.6 (6) |
| P | 1118 (2) | 3148 (2) | 1132 (1) | 42.2 (7) |
| O(1) | 1860 (8) | −1178 (6) | 4296 (5) | 83 (3) |
| O(2) | 1315 (10) | 1514 (7) | 6344 (5) | 97 (4) |
| O(3) | −793 (7) | 1226 (7) | 3765 (6) | 92 (4) |
| O(4) | 4074 (10) | −1463 (7) | 2819 (7) | 115 (4) |
| O(5) | 581 (10) | −444 (8) | 1800 (6) | 119 (4) |
| O(6) | 4772 (9) | 663 (8) | 1265 (6) | 112 (4) |
| O(7) | 5654 (15) | 2741 (9) | 5846 (8) | 189 (7) |
| O(8) | 5511 (9) | 3341 (9) | 3242 (8) | 137 (6) |
| O(9) | 6314 (9) | 214 (12) | 3660 (10) | 178 (8) |
| O(10) | 2940 (18) | 3703 (11) | 6589 (7) | 203 (9) |
| O(11) | 3456 (13) | 5241 (8) | 4510 (8) | 147 (6) |
| O(12) | −535 (13) | 3807 (8) | 4982 (10) | 170 (7) |
| C(1) | 1910 (9) | −309 (7) | 4305 (6) | 54 (3) |
| C(2) | 1561 (11) | 1416 (8) | 5597 (7) | 70 (4) |
| C(3) | 273 (9) | 1178 (8) | 4024 (6) | 61 (4) |
| C(4) | 3630 (10) | −611 (9) | 2844 (7) | 73 (4) |
| C(5) | 1508 (11) | 7 (8) | 2178 (7) | 68 (4) |
| C(6) | 4024 (11) | 691 (9) | 1813 (8) | 79 (5) |
| C(7) | 5058 (15) | 2435 (11) | 5243 (11) | 117 (7) |
| C(8) | 5003 (11) | 2798 (12) | 3609 (10) | 109 (7) |
| C(9) | 5482 (10) | 859 (13) | 3848 (11) | 110 (7) |
| C(10) | 2736 (20) | 3446 (13) | 5820 (8) | 140 (8) |
| C(11) | 2987 (15) | 4459 (11) | 4562 (8) | 106 (6) |
| C(12) | 555 (16) | 3608 (10) | 4896 (10) | 118 (7) |
| C(21) | 2304 (13) | 5064 (8) | 2084 (8) | 87 (5) |
| C(22) | 2249 (20) | 6177 (11) | 2523 (9) | 131 (8) |
| C(23) | 1056 (26) | 6730 (12) | 2551 (11) | 154 (10) |
| C(24) | −27 (18) | 6260 (13) | 2143 (9) | 142 (8) |
| C(25) | −11 (13) | 5183 (9) | 1699 (6) | 78 (4) |
| C(26) | 1179 (10) | 4589 (8) | 1661 (5) | 56 (3) |
| C(27) | 3636 (12) | 4523 (9) | 2033 (10) | 109 (6) |
| C(31) | 2390 (13) | 1968 (10) | −438 (7) | 88 (5) |
| C(32) | 3116 (16) | 1911 (13) | −1250 (8) | 121 (7) |
| C(33) | 3523 (16) | 2809 (17) | −1473 (11) | 160 (10) |
| C(34) | 3247 (14) | 3742 (14) | −977 (10) | 117 (7) |
| C(35) | 2509 (10) | 3881 (9) | −168 (7) | 69 (4) |
| C(36) | 2061 (9) | 2978 (8) | 95 (5) | 53 (3) |
| C(37) | 1902 (14) | 951 (10) | −251 (7) | 101 (6) |
| C(41) | −1594 (12) | 2778 (15) | 1395 (11) | 128 (8) |
| C(42) | −2880 (14) | 2554 (20) | 1048 (17) | 199 (15) |
| C(43) | −3213 (18) | 2556 (15) | 182 (18) | 153 (13) |
| C(44) | −2279 (15) | 2667 (11) | −388 (11) | 108 (7) |
| C(45) | −964 (11) | 2838 (9) | −101 (7) | 76 (4) |
| C(46) | −615 (9) | 2886 (8) | 782 (6) | 61 (4) |
| C(47) | −1287 (14) | 2919 (19) | 2395 (11) | 232 (16) |
| B | 2487 (9) | 2032 (7) | 3546 (6) | 43 (3) |

[a] Equivalent isotropic *U* defined as one-third of the trace of the orthogonalized $U_{ij}$ tensor.

**Molecular Structure of 1.** The molecular structure of **1** is shown in Figure 1, and selected bond distances and angles are collected in Table III. The structure is, as expected, related directly to that of the parent compound $HFe_4(CO)_{12}BH_2$[22,23] by the replacement of one bridging hydrogen atom by the AuP(2-Me-$C_6H_4$)$_3$ group and is thereby consistent with the isolobal principle.[24,25] The present determination of the structure of **1** confirms an earlier proposal made for $HFe_4(CO)_{12}BHAuPPh_3$.[3] The internal dihedral angle of the $Fe_4$ butterfly framework is 114.6° in **1** compared to 114.0° in $HFe_4(CO)_{12}BH_2$[22,23] and

(22) Wong, K. S.; Scheidt, W. R.; Fehlner, T. P. *J. Am. Chem. Soc.* **1982**, *104*, 1111.
(23) Fehlner, T. P.; Housecroft, C. E.; Scheidt, W. R.; Wong, K. S. *Organometallics* **1983**, *2*, 825.
(24) Lauher, J. W.; Wald, K. *J. Am. Chem. Soc.* **1981**, *103*, 7648.
(25) Hall, K. P.; Mingos, D. M. P. *Prog. Inorg. Chem.* **1984**, *32*, 237.

**Table III. Selected Bond Distances (Å) and Angles (deg) for 1**

(a) Bond Distances

| | | | |
|---|---|---|---|
| Au-Fe(2) | 2.580 (1) | Au-P | 2.321 (2) |
| Au-B | 2.310 (10) | Fe(1)-Fe(2) | 2.680 (2) |
| Fe(1)-Fe(3) | 2.604 (2) | Fe(1)-Fe(4) | 2.652 (2) |
| Fe(2)-Fe(3) | 2.675 (2) | Fe(1)-B | 2.056 (11) |
| Fe(3)-Fe(4) | 2.663 (2) | Fe(2)-B | 1.964 (9) |
| Fe(3)-B | 2.048 (9) | Fe(4)-B | 2.008 (8) |
| P-C(26) | 1.827 (9) | P-C(36) | 1.815 (8) |
| P-C(46) | 1.819 (9) | | |

(b) Bond Angles

| | | | |
|---|---|---|---|
| Fe(2)-Au-P | 163.9 (1) | Fe(2)-Au-B | 47.0 (2) |
| P-Au-B | 149.2 (2) | Fe(2)-Fe(1)-Fe(3) | 60.8 (1) |
| Fe(2)-Fe(1)-Fe(4) | 94.6 (1) | Fe(3)-Fe(1)-Fe(4) | 60.9 (1) |
| Fe(2)-Fe(1)-B | 46.7 (2) | Fe(3)-Fe(1)-B | 50.5 (2) |
| Fe(4)-Fe(1)-B | 48.5 (2) | Au-Fe(2)-Fe(1) | 101.2 (1) |
| Au-Fe(2)-Fe(3) | 98.6 (1) | Fe(1)-Fe(2)-Fe(3) | 58.2 (1) |
| Au-Fe(2)-B | 59.3 (3) | Fe(1)-Fe(2)-B | 49.7 (3) |
| Fe(3)-Fe(2)-B | 49.5 (3) | Fe(1)-Fe(3)-Fe(2) | 61.0 (1) |
| Fe(1)-Fe(3)-Fe(4) | 60.5 (1) | Fe(2)-Fe(3)-Fe(4) | 94.4 (1) |
| Fe(1)-Fe(3)-B | 50.8 (3) | Fe(2)-Fe(3)-B | 46.8 (2) |
| Fe(4)-Fe(3)-B | 48.3 (2) | Fe(1)-Fe(4)-Fe(3) | 58.7 (1) |
| Fe(1)-Fe(4)-B | 50.1 (3) | Fe(3)-Fe(4)-B | 49.6 (3) |
| Au-B-Fe(1) | 137.1 (4) | Au-B-Fe(2) | 73.8 (3) |
| Fe(1)-B-Fe(2) | 83.6 (4) | Au-B-Fe(3) | 132.2 (4) |
| Fe(1)-B-Fe(3) | 78.8 (4) | Au-B-Fe(4) | 125.2 (5) |
| Fe(2)-B-Fe(3) | 83.6 (3) | Fe(1)-B-Fe(4) | 81.4 (4) |
| Fe(2)-B-Fe(4) | 161.0 (6) | Fe(3)-B-Fe(4) | 82.1 (3) |
| Au-P-C(26) | 111.4 (3) | Au-P-C(36) | 113.3 (3) |
| Au-P-C(46) | 115.4 (4) | | |

the boron atom is 0.33 Å above the $Fe_{wingtip}\cdots Fe_{wingtip}$ vector (viz. Fe(2)---Fe(4)) compared to 0.31 Å in the parent compound. In $HFe_4(CO)_{12}BH_2$, the boron atom is symmetrically placed between the two wingtip iron atoms (Fe–B = 1.966 (6) and 1.974 (6) Å),[22,23] whereas in 1, the edge bridged by the hydrogen atom is slightly longer than that bridged by the gold(I) phosphine fragment (2.008 (8) versus 1.964 (9) Å). On the whole, however, the introduction of the heavy-metal unit causes little perturbation either to the $Fe_4B$ cluster core or to the arrangement of the 12 carbonyl ligands.

Replacement of a boron-attached bridging hydrogen atom by an {AuP(2-Me-$C_6H_4$)$_3$} fragment has been observed in the reaction of MeAuP(2-Me-$C_6H_4$)$_3$ with $B_{10}H_{14}$, and the structural characterization of the resultant auraborane $B_{10}H_{13}$AuP(2-Me-$C_6H_4$)$_3$ reveals distances of Au–B = 2.256 (15) and 2.325 (16) Å and B–B = 1.745 (22) Å for the B–Au{P(2-Me-$C_6H_4$)$_3$}–B bridging unit.[26] These values compare with parameters for the three-center two-electron AuBFe bridging unit in 1 of B–Au = 2.310 (10) Å, Au–Fe(2) = 2.580 (1) Å, and Fe(2)–B = 1.964 (9) Å. The angle subtended at the gold atom is ∠B–Au–B = 44.8 (5)° in the auraborane[26] and ∠B–Au–Fe(2) = 47.0 (2) Å in 1. Gold–phosphorus distances compare as follows: 2.308 (3) Å in $B_{10}H_{13}$AuP(2-Me-$C_6H_4$)$_3$[26] and 2.321 (2) Å in 1. The structure of the gold(I) precursor (2-Me-$C_6H_4$)$_3$PAuCl has only recently been determined,[27] and a comparison of selected characteristic geometrical parameters for this and for corresponding values in 1 is given in Table IV. Apart from an increase in the Au–P bond length, there are no significant changes in the geometry of the {(2-Me-$C_6H_4$)$_3$PAu} fragment upon association with the cluster.

Cluster hydrides were not located but may be inferred from $^1$H NMR spectroscopic data to be Fe–H–B and Fe–H–Fe bridging by nature. An inspection of the carbonyl ligand orientations illustrates that vectors O(8)C(8)Fe(3) and O(3)C(3)Fe(1) point toward a common vacancy in the approximately octahedral coordination sphere of atoms Fe(1) and Fe(3). Similarly, extending the vector O(10)C(10)Fe(4) leads to a coordination vacancy on atom Fe(4). Thus, we propose that the hydride ligands bridge edges Fe(1)–Fe(3) and Fe(4)–B as shown in structure I.

**Table IV. Comparison of the Geometrical Parameters of the AuP(2-Me-$C_6H_4$)$_3$ Group in the Chloride and in 1**

| | (2-Me-$C_6H_4$)$_3$PAuCl[27] | 1 |
|---|---|---|
| | Distances (Å) | |
| Au-P | 2.243 (2) | 2.312 (2) |
| | Angles (deg) | |
| X-Au-P[a] | 179.4 (1) | 174.1 |
| Au-P-$C_{ipso}$ | 112.8 (3) | 111.4 (3) |
| | 114.5 (3) | 113.3 (3) |
| | 114.2 (3) | 115.4 (4) |
| $C_{ipso}$-P-$C_{ipso}$ | 104.7 (4) | 105.9 (4) |
| | 105.6 (4) | 105.4 (4) |
| | 104.1 (4) | 104.5 (4) |

[a] X = Cl or (for 1) the midpoint of Fe(2)–B.

**Deprotonation of 1 and 2.** Treatment of 1 with $Et_3N$ leads to the formation of $[Et_3NH][1]$ in ~95% yield. In the $^1$H NMR spectrum, 1 exhibits a broad resonance at δ −7.7 and a sharp signal at δ −24.9 assigned to the Fe–H–B and Fe–H–Fe bridges, respectively. Upon addition of amine, both resonances disappear and a new signal, a collapsed quartet at δ −9.4, emerges. In the $^{11}$B NMR spectrum, only a small shift from δ +136.0 for 1 to δ 137.0 for $[Et_3NH][1]$ is observed; this implies a similar environment for the boron atom in each cluster.[28] Both the $^1$H and $^{11}$B NMR data are therefore consistent with the removal of a proton from the Fe–H–Fe site. This mimics the pattern of deprotonation for $HFe_4(CO)_{12}BH_2$ in which the sequence is loss of Fe–H–B followed by Fe–H–Fe.[29] In our case, the loss of a single proton from 1 is considered to be analogous to the loss of the second proton from $HFe_4(CO)_{12}BH_2$.

When $^n$BuLi is added to 1, deprotonation to give Li[1] does not occur. Instead, alkylation of the gold(I) phosphine group is observed as shown in eq 1. The ferraborane

$$HFe_4(CO)_{12}BHAuP(2\text{-Me-}C_6H_4)_3 + Li^nBu \rightarrow Li[HFe_4(CO)_{12}BH] + {}^n\text{BuAuP}(2\text{-Me-}C_6H_4)_3 \quad (1)$$

product was characterized by comparing its spectroscopic properties with those previously reported for salts of $[HFe_4(CO)_{12}BH]^-$.[29-31] The reaction of 1 with $^n$BuLi therefore parallels the alkylation of LAuCl (L = phosphine ligand), first documented by Coates et al.[32]

In contrast to 1, 2 deprotonates by loss of an Ru–H–B bridging hydrogen atom. The high-field region of the $^1$H NMR spectrum of $[Et_3NH][2]$ consists of a single sharp resonance at δ −20.9. In the $^{11}$B NMR spectrum, a shift in the resonance from δ +132.1 to +171.4 accompanies deprotonation and this implies a significant change in the environment of the boron atom and an increase in the degree of direct boron to metal interaction. The difference in deprotonations of 1 and 2 is consistent with the differences in deprotonations of the parent clusters $HFe_4(CO)_{12}BH_2$ and $HRu_4(CO)_{12}BH_2$.[29,33]

**Formation of the Fused Cluster Anions $[\{HM_4(CO)_{12}BH\}_2Au]^-$ ([4]$^-$, M = Fe; [5]$^-$, M = Ru).** The

(26) Wynd, A. J.; McLennan, A. J.; Reed, D.; Welch, A. J. *J. Chem. Soc., Dalton Trans.* **1987**, 2761.
(27) Harker, C. S. W.; Tiekink, E. R. T. *Acta Crystallogr., Sect. C* **1990**, *46*, 1546.
(28) Rath, N. P.; Fehlner, T. P. *J. Am. Chem. Soc.* **1988**, *110*, 5345.
(29) Rath, N. P.; Fehlner, T. P. *J. Am. Chem. Soc.* **1987**, *109*, 5273.
(30) Housecroft, C. E.; Buhl, M. L.; Long, G. J.; Fehlner, T. P. *J. Am. Chem. Soc.* **1987**, *109*, 3323.
(31) Housecroft, C. E.; Fehlner, T. P. *Organometallics* **1986**, *5*, 379.
(32) Calvin, G.; Coates, G. E.; Dixon, P. S. *Chem. Ind.* **1959**, 1628.
(33) Hong, F.-E.; McCarthy, D. A.; White, J. P.; Cottrell, C. E.; Shore, S. G. *Inorg. Chem.* **1990**, *29*, 2874.

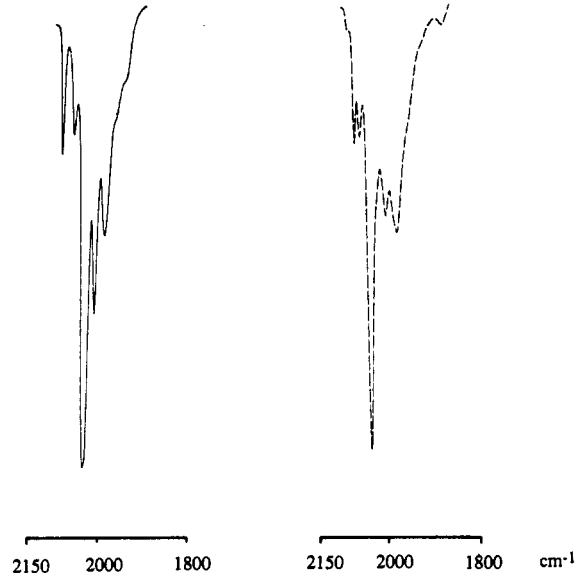


**Figure 2.** Comparison of the infrared spectra ($\nu_{CO}$ only) of (a) 1 and (b) $[4]^-$.

formation of 1 may only be achieved if a carefully controlled 1:1 reaction between $[HFe_4(CO)_{12}BH]^-$ and (2-Me-$C_6H_4)_3$PAuCl is carried out. In the presence of >1 molar equiv of the gold(I) phosphine, a competitive pathway involving Au–P bond cleavage becomes significant. With an approximately 3-fold excess of (2-Me-$C_6H_4)_3$PAuCl, the yield of 1 is reduced to ~30% and the major product, obtained in ~50% yield, is [Au{P(2-Me-$C_6H_4)_3$}$_2$][{$HFe_4(CO)_{12}BH$}$_2$Au] ([Au{P(2-Me-$C_6H_4)_3$}$_2$][4]). The cluster anion $[4]^-$ is produced as a result of Au–P bond cleavage.[6] A similar pathway is followed in reactions of $[HFe_4(CO)_{12}BH]^-$ with LAuCl where L = $PEt_3$, $PMe_3$, $PPhMe_2$, and $PPh_2Me$.[6] However, in these cases this pathway competes not with the formation of the monogold but with that of the digold derivative[7] and $[AuL_2][4]$ is not a predominant product.

We have also studied the reaction of ClAu(dppm)AuCl with [PPN][$HFe_4(CO)_{12}BH$]. The dppm ligand is small enough[7] to bridge over the top of the $Fe_4B$ butterfly core, and $HFe_4(CO)_{12}BAu_2$(dppm) (6) is formed in ~40% yield. Compound 6 is a digold derivative of type IIa. However, the pathway to the fused anion $[4]^-$ is also favorable and $[4]^-$ forms in ~30% yield. Note that, in this case, the counterion is $[PPN]^+$ rather than the bis(phosphine)gold(I) cation as in the reactions with monodentate phosphines described above.

The ruthenium analog of $[4]^-$, $[5]^-$, may be prepared in 40% yield as its $[PPN]^+$ salt via the reaction of [PPN]-[$HRu_4(CO)_{12}BH$] with ClAu(dppm)AuCl. Both $[4]^-$ and $[5]^-$ possess $^{11}B$ and $^1H$ NMR spectral signatures that closely resemble those of compounds 1 and 2, respectively. The $^{11}B$ NMR resonance for $[4]^-$ of $\delta$ +134.0 is close to that of 1 ($\delta$ +136.0), and that of $[5]^-$ ($\delta$ +133.9) compares favorably with that of 2 ($\delta$ +132.1). Similarly, $^1H$ NMR data for $[4]^-$ are similar to those of 1 ($\delta$ –6.4 (Fe–*H*–B) and –24.9 (Fe–*H*–Fe) versus $\delta$ –7.7 (Fe–*H*–B) and –24.9 (Fe–*H*–Fe), respectively) and shift values for $[5]^-$ are comparable to those of 2 ($\delta$ –4.1 (Ru–*H*–B) and –20.9 (Ru–*H*–Ru) versus $\delta$ –4.7 (Ru–*H*–B) and –20.8 (Ru–*H*–Ru), respectively). The infrared spectrum in the carbonyl region of $[4]^-$ is very similar to that of 1 (Figure 2) and similarly for $[5]^-$ and 2. Only the fact that the clusters were anionic as opposed

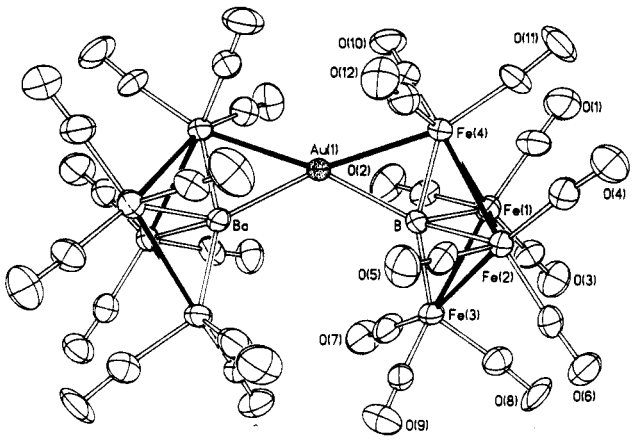


**Figure 3.** Molecular structure of $[4]^-$ determined for the [Au-($PMePh_2$)$_2$]$^+$ salt (see text). The anion is disordered, with the gold atom occupying two chemically equivalent sites. Only one occupancy is depicted in the figure. Hydrogen atoms were not located.

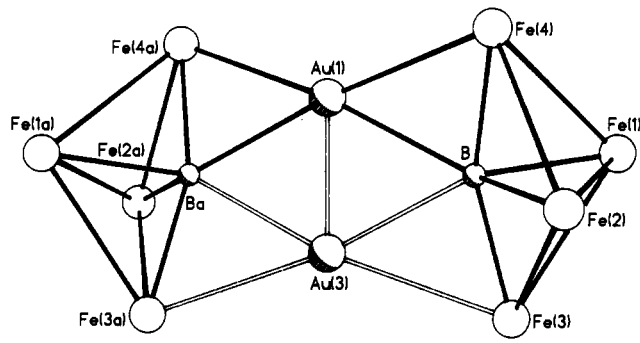


**Figure 4.** Core structure of $[4]^-$ showing the two chemically equivalent sites of the gold atoms.

to being neutral suggested the possibility of their fused nature. This was confirmed by FAB mass spectral data and definitively so by X-ray diffraction studies of [Au-{$PMePh_2$}$_2$][4] and [PPN][5].

**Molecular Structure of [Au{$PMePh_2$}$_2$][4].** The molecular structure of the anion $[4]^-$ is presented in Figure 3, and selected bond distances and angles are listed in Table VI. The structure consists of two {$HFe_4(CO)_{12}BH$} fragments fused in a "face-to-face" manner via a single gold atom which bridges one $Fe_{wingtip}$–B edge of each cluster unit. The geometry of each butterfly fragment varies little from that described above for compound 1; the bridging Au(P(2-Me-$C_6H_4)_3$) ligand of 1 is replaced in $[4]^-$ by the bridging Au atom.

The internal dihedral angle of the $Fe_4$ skeleton is 116.6 (3)° in $[4]^-$ compared to 114.6° in 1, and the boron atom lies 0.39 Å above the $Fe_{wingtip}$–$Fe_{wingtip}$ axis compared to 0.33 Å in 1. The anion contains two chemically equivalent Au atom sites (Figure 4), with occupancies of 0.402 (1) for Au(1) and 0.098 (1) for Au(3). Hydrogen atoms were not located, but from NMR spectroscopic data and from an inspection of the carbonyl ligand orientations we propose that they bridge edges Fe(1)–Fe(2) and Fe(3)–B (or Fe(4)–B). As in 1, the gold-bridged Fe–B edge is shorter than the hydrogen-bridged edge in $[4]^-$ with Fe(2)–B = 2.082 (12) Å and Fe(4)–B = 1.990 (12) Å.

Figure 3 illustrates that the two {$HFe_4(CO)_{12}BH$} units reside in a mutually cis arrangement with respect to coordination about the gold(I) center. (This description is for convenience only and does not imply that the geometry about the gold(I) atom should be considered as being square planar; see below.) The two cluster subunits are twisted with respect to one another with a spiro twist angle

**Table V. Atomic Coordinates (×10⁴) and Isotropic Thermal Parameters (Å² × 10³) for $[Au(PMePh_2)_2][4]$**

| | x | y | z | U[a] |
|---|---|---|---|---|
| Au(1) | 0 | 7090.4 (7) | 2500 | 44.1 (3)* |
| Au(2) | 2500 | 7500 | 0 | 71.0 (3)* |
| Fe(1) | 1124.6 (7) | 7881 (2) | 3651.9 (6) | 54.0 (6)* |
| Fe(2) | 1704.5 (7) | 8620 (2) | 2965.3 (5) | 48.3 (5)* |
| Fe(3) | 788.1 (7) | 10196 (2) | 3192.6 (6) | 54.3 (6)* |
| Fe(4) | 1062.7 (7) | 6229 (2) | 2926.3 (5) | 49.4 (6)* |
| Au(3) | 0 | 9295 (3) | 2500 | 42 (1)* |
| P | 1727 (2) | 7022 (4) | 439 (1) | 64 (1)* |
| O(1) | 1674 (5) | 5461 (11) | 4134 (4) | 118 (5)* |
| O(2) | -167 (5) | 7279 (12) | 3749 (4) | 114 (5)* |
| O(3) | 1394 (5) | 9511 (11) | 4484 (3) | 99 (4)* |
| O(4) | 2834 (5) | 7025 (10) | 2876 (4) | 100 (5)* |
| O(5) | 1355 (4) | 9041 (11) | 1987 (3) | 87 (4)* |
| O(6) | 2473 (4) | 11121 (9) | 3128 (3) | 81 (4)* |
| O(7) | -341 (4) | 10940 (11) | 3593 (4) | 108 (5)* |
| O(8) | 1571 (4) | 12008 (10) | 3834 (4) | 99 (4)* |
| O(9) | 794 (5) | 12254 (9) | 2453 (3) | 90 (4)* |
| O(10) | 224 (4) | 4119 (9) | 3233 (3) | 93 (4)* |
| O(11) | 2150 (4) | 4472 (11) | 3201 (4) | 111 (5)* |
| O(12) | 1110 (4) | 5407 (11) | 1988 (3) | 90 (4)* |
| C(1) | 1468 (7) | 6376 (13) | 3932 (4) | 75 (5)* |
| C(2) | 328 (6) | 7517 (12) | 3707 (4) | 67 (5)* |
| C(3) | 1292 (6) | 8904 (13) | 4154 (4) | 66 (5)* |
| C(4) | 2373 (6) | 7597 (13) | 2913 (5) | 69 (5)* |
| C(5) | 1490 (5) | 8900 (13) | 2368 (4) | 66 (5)* |
| C(6) | 2157 (5) | 10188 (12) | 3070 (4) | 59 (4)* |
| C(7) | 91 (6) | 10647 (14) | 3431 (5) | 81 (6)* |
| C(8) | 1284 (5) | 11250 (13) | 3585 (4) | 66 (5)* |
| C(9) | 781 (5) | 11462 (12) | 2734 (4) | 64 (5)* |
| C(10) | 543 (5) | 4937 (12) | 3109 (4) | 66 (5)* |
| C(11) | 1751 (6) | 5185 (13) | 3116 (4) | 70 (5)* |
| C(12) | 1079 (5) | 5716 (13) | 2353 (4) | 66 (5)* |
| B | 767 (5) | 8189 (13) | 2981 (5) | 49 (4)* |
| C(21) | 1791 (7) | 8108 (14) | 940 (5) | 87 (6)* |
| C(22) | 774 (9) | 6543 (18) | -247 (6) | 136 (12) |
| C(23) | 177 | 6741 | -476 | 182 (17) |
| C(24) | -214 | 7743 | -321 | 197 (19) |
| C(25) | -8 | 8546 | 61 | 227 (22) |
| C(26) | 589 | 8347 | 289 | 188 (18) |
| C(27) | 980 | 7346 | 135 | 106 (5) |
| C(28) | 2038 (4) | 4179 (11) | 409 (3) | 93 (7)* |
| C(29) | 2044 | 2797 | 563 | 108 (8)* |
| C(30) | 1748 | 2451 | 938 | 91 (7)* |
| C(31) | 1447 | 3487 | 1159 | 106 (8)* |
| C(32) | 1442 | 4868 | 1005 | 87 (6)* |
| C(33) | 1737 | 5214 | 630 | 64 (5)* |

[a] Asterisks denote equivalent isotropic $U$ values, defined as one-third of the trace of the orthogonalized $U_{ij}$ tensor.

**Table VI. Selected Bond Distances (Å) and Angles (deg) for $[4]^-$**

(a) Bond Distances

| | | | |
|---|---|---|---|
| Fe(4)-Au(1) | 2.615 (1) | Au(1)-B | 2.300 (12) |
| Fe(1)-Fe(2) | 2.630 (2) | Fe(1)-Fe(3) | 2.649 (2) |
| Fe(1)-Fe(4) | 2.660 (2) | Fe(2)-Fe(3) | 2.650 (2) |
| Fe(2)-Fe(4) | 2.668 (2) | Fe(1)-B | 2.065 (13) |
| Fe(2)-B | 2.082 (12) | Fe(3)-B | 2.015 (12) |
| Fe(4)-B | 1.990 (12) | | |

(b) Bond Angles

| | | | |
|---|---|---|---|
| Fe(4)-Au(1)-B | 47.2 (3) | Fe(4)-Au(1)-Fe(4a) | 143.4 (1) |
| B-Au(1)-Fe(4a) | 164.9 (3) | B-Au(1)-B(a) | 125.8 (6) |
| Fe(2)-Fe(1)-Fe(3) | 60.3 (1) | Fe(2)-Fe(1)-Fe(4) | 60.6 (1) |
| Fe(3)-Fe(1)-Fe(4) | 95.5 (1) | Fe(2)-Fe(1)-B | 50.9 (3) |
| Fe(2)-Fe(1)-B | 48.7 (3) | Fe(4)-Fe(1)-B | 47.8 (3) |
| Fe(1)-Fe(2)-Fe(3) | 60.2 (1) | Fe(1)-Fe(2)-Fe(4) | 60.3 (1) |
| Fe(3)-Fe(2)-Fe(4) | 95.2 (1) | Fe(1)-Fe(2)-B | 50.4 (4) |
| Fe(3)-Fe(2)-B | 48.6 (3) | Fe(4)-Fe(2)-B | 47.6 (3) |
| Fe(1)-Fe(3)-Fe(2) | 59.5 (1) | Fe(1)-Fe(3)-B | 50.3 (4) |
| Fe(2)-Fe(3)-B | 50.8 (3) | Au(1)-Fe(4)-Fe(1) | 98.9 (1) |
| Au(1)-Fe(4)-Fe(2) | 100.1 (1) | Fe(1)-Fe(4)-Fe(2) | 59.1 (1) |
| Au(1)-Fe(4)-B | 58.0 (3) | Fe(1)-Fe(4)-B | 50.2 (4) |
| Fe(2)-Fe(4)-B | 50.6 (3) | Au(1)-B-Fe(1) | 133.3 (6) |
| Au(1)-B-Fe(2) | 135.0 (7) | Fe(1)-B-Fe(2) | 78.7 (4) |
| Au(1)-B-Fe(3) | 127.8 (5) | Fe(1)-B-Fe(3) | 81.0 (5) |
| Fe(2)-B-Fe(3) | 80.6 (4) | Au(1)-B-Fe(4) | 74.7 (4) |
| Fe(1)-B-Fe(4) | 82.0 (5) | Fe(2)-B-Fe(4) | 81.8 (4) |
| Fe(3)-B-Fe(4) | 157.5 (6) | | |

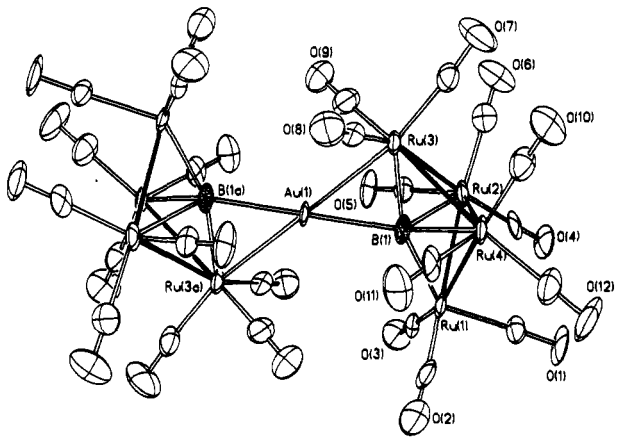


**Figure 5.** Molecular structure of $[5]^-$ determined for the $[PPN]^+$ salt. Hydrogen atoms were not located. One of the two chemically similar but crystallographically different independent anions is shown.

of 30.9 (5)° at the gold atom. The origin of this twist presumably arises from the close proximity of pairs of carbonyl ligands on the two cluster units, since nonbonded CO···O(a)C(a) interactions are at a maximum when atoms Fe(4), B, Au(1), B(a), and Fe(4a) are coplanar. This point will be addressed further below.

The phosphine ligands in the $[AuL_2]^+$ cations are a mixture of $PMePh_2$ and $PMe_2Ph$ molecules. Occupancy refinement shows $PMePh_2$ to be present as a 63 (1)% component of the mixture. The geometry of the cation is unexceptional with linear coordination at the gold(I) center ∠P-Au-P = 180.0 (1)°. Each Au-P bond length is 2.300 (4) Å. There are no significant cation-anion interactions.

**Molecular Structure of [PPN][5].** The molecular structure of $[5]^-$ is given in Figure 5, and selected bond distances and angles are listed in Table VIII. Two chemically similar, but crystallographically independent, half-anions are situated on inversion centers. Thus, the anion comprises two inversionally related cluster subunits, fused via a gold atom in a "face-to-face" orientation and in a mutually trans configuration with atom Au(1) lying on a crystallographic inversion center (as with $[4]^-$, the use of the descriptor trans is given for convenience only and does not imply that the Au(I) atom is in a formal square-planar environment; see discussion below). The gold atom bridges one $Ru_{wingtip}$-B edge of each cluster unit. The structure of each $[Ru_4(CO)_{12}B]$ subunit is similar to that of both the parent ruthenaborane $HRu_4(CO)_{12}BH_2$[33] and of $HRu_4(CO)_{12}BAu_2(PPh_3)_2$.[8] The internal dihedral angle of the $Ru_4$ butterfly is 116.1° (average) in $[5]^-$ compared to 118° in $HRu_4(CO)_{12}BH_2$[33] and 117.4° in $HRu_4(CO)_{12}BAu_2(PPh_3)_2$.[8] The boron atom is displaced above the $Ru_{wingtip}$-$Ru_{wingtip}$ axis (viz, Ru(1)···Ru(3) in Figure 5) by 0.375 Å (average) in $[5]^-$ compared to 0.39 Å in $HRu_4(CO)_{12}BH_2$[33] and 0.37 Å in $HRu_4(CO)_{12}BAu_2(PPh_3)_2$.[8] Thus, as observed previously for the $Fe_4B$ core in related auraferraboranes,[19] the $Ru_4B$ cluster core appears to be resistant to structural change as cluster-bound hydrogen atoms are replaced by one or more gold(I) phosphine fragments.

Hydrogen atoms were not located in $[5]^-$, but as in 1 and $[4]^-$, NMR spectroscopic data and an inspection of the orientations of the carbonyl ligands show that each cluster subunit possesses two hydrogen atoms bridging edges Ru(2)-Ru(4) and Ru(1)-B(1), respectively. In the parent cluster $HRu_4(CO)_{12}BH_2$, the two $Ru_{wingtip}$-B edges, viz.

**Table VII. Atomic Coordinates (×10⁴) and Isotropic Thermal Parameters (Å² × 10³) for [PPN][5]**

| | x | y | z | U[a] | | x | y | z | U[a] |
|---|---|---|---|---|---|---|---|---|---|
| Ru(1) | 7335.9 (14) | 4200.4 (10) | 872.8 (5) | 39.9 (5)* | C(12) | 8960 (22) | 3973 (16) | 1999 (7) | 67 (9)* |
| Ru(2) | 8848.0 (15) | 2568.8 (9) | 579.7 (5) | 37.7 (5)* | C(13) | −823 (25) | 4803 (16) | 3866 (8) | 73 (9)* |
| Ru(3) | 11311.4 (14) | 3695.7 (10) | 535.4 (5) | 35.5 (5)* | C(14) | 1471 (22) | 4092 (16) | 3455 (7) | 66 (8)* |
| Ru(4) | 9952.3 (15) | 3973.1 (10) | 1416.0 (5) | 39.5 (5)* | C(15) | 2008 (20) | 5543 (13) | 4280 (8) | 61 (8)* |
| Ru(5) | 902.3 (16) | 4334.0 (10) | 4118.7 (5) | 44.3 (5)* | C(16) | 3626 (20) | 4071 (14) | 5077 (7) | 55 (7)* |
| Ru(6) | 2883.7 (15) | 3100.6 (10) | 4558.6 (5) | 38.9 (5)* | C(17) | 4153 (22) | 2139 (15) | 4776 (8) | 65 (8)* |
| Ru(7) | 1043.4 (16) | 2330.5 (10) | 5154.5 (5) | 42.6 (5)* | C(18) | 3947 (18) | 3522 (12) | 4066 (7) | 48 (7)* |
| Ru(8) | 163.5 (16) | 2321.5 (10) | 4113.6 (5) | 45.6 (5)* | C(19) | 1671 (22) | 1040 (14) | 5055 (7) | 61 (8)* |
| Au(1) | 10000 | 5000 | 0 | 33.6 (3)* | C(20) | 2222 (24) | 2624 (14) | 5777 (8) | 69 (9)* |
| Au(2) | 0 | 5000 | 5000 | 42.5 (4)* | C(21) | −603 (25) | 1029 (13) | 5398 (7) | 69 (9)* |
| P(1) | 3070 (5) | 9332 (3) | 1907 (2) | 41 (2)* | C(22) | 11 (21) | 937 (15) | 4073 (8) | 71 (8)* |
| P(2) | 3172 (5) | 7965 (4) | 2691 (2) | 47 (2)* | C(23) | −144 (26) | 2304 (15) | 3402 (8) | 83 (10)* |
| N | 3255 (17) | 8399 (10) | 2171 (5) | 51 (6)* | C(24) | −1716 (24) | 2545 (15) | 4217 (8) | 73 (9)* |
| B(1) | 9307 (24) | 4135 (13) | 619 (7) | 46 (8)* | C(31) | 3446 (11) | 9673 (7) | 945 (4) | 49 (5) |
| B(2) | 811 (23) | 3541 (13) | 4711 (7) | 43 (7)* | C(32) | 4020 | 9496 | 497 | 60 (5) |
| O(1) | 5821 (16) | 3165 (11) | 1600 (5) | 82 (7)* | C(33) | 4966 | 8772 | 442 | 62 (5) |
| O(2) | 6742 (16) | 6208 (10) | 1375 (6) | 84 (7)* | C(34) | 5338 | 8224 | 836 | 63 (5) |
| O(3) | 4929 (14) | 3823 (10) | 4 (5) | 71 (6)* | C(35) | 4765 | 8401 | 1284 | 48 (4) |
| O(4) | 6366 (14) | 1349 (9) | 812 (5) | 69 (6)* | C(36) | 3819 | 9126 | 1339 | 39 (4) |
| O(5) | 7999 (15) | 2637 (10) | −536 (4) | 67 (6)* | C(41) | 783 (12) | 10489 (7) | 1808 (5) | 60 (5) |
| O(6) | 10644 (17) | 843 (10) | 414 (6) | 90 (7)* | C(42) | −628 | 10618 | 1688 | 82 (7) |
| O(7) | 13247 (16) | 2170 (10) | 935 (7) | 93 (7)* | C(43) | −1530 | 9817 | 1514 | 77 (6) |
| O(8) | 13447 (14) | 5384 (10) | 817 (5) | 70 (6)* | C(44) | −1023 | 8889 | 1459 | 88 (7) |
| O(9) | 11729 (16) | 3000 (10) | −546 (5) | 76 (6)* | C(45) | 387 | 8761 | 1579 | 72 (6) |
| O(10) | 12607 (15) | 3269 (13) | 1967 (6) | 93 (7)* | C(46) | 1290 | 9561 | 1754 | 50 (5) |
| O(11) | 10674 (17) | 6140 (10) | 1550 (6) | 84 (7)* | C(51) | 5119 (13) | 10805 (9) | 2142 (4) | 72 (6) |
| O(12) | 8459 (18) | 4024 (13) | 2342 (5) | 98 (8)* | C(52) | 5815 | 11598 | 2445 | 84 (7) |
| O(13) | −1912 (18) | 5030 (14) | 3713 (6) | 106 (8)* | C(53) | 5291 | 11997 | 2877 | 82 (7) |
| O(14) | 1812 (19) | 3985 (14) | 3068 (5) | 107 (8)* | C(54) | 4070 | 11605 | 3006 | 90 (7) |
| O(15) | 2646 (19) | 6217 (10) | 4379 (7) | 106 (8)* | C(55) | 3374 | 10813 | 2702 | 73 (6) |
| O(16) | 4045 (16) | 4651 (11) | 5401 (5) | 86 (7)* | C(56) | 3898 | 10413 | 2270 | 50 (5) |
| O(17) | 4899 (17) | 1629 (11) | 4939 (7) | 94 (7)* | C(61) | 4059 (15) | 6296 (9) | 2200 (4) | 67 (6) |
| O(18) | 4664 (14) | 3739 (10) | 3788 (5) | 69 (6)* | C(62) | 4614 | 5382 | 2177 | 88 (7) |
| O(19) | 2042 (19) | 262 (10) | 4991 (6) | 94 (7)* | C(63) | 5073 | 4994 | 2620 | 92 (8) |
| O(20) | 3001 (20) | 2778 (13) | 6142 (5) | 108 (8)* | C(64) | 4976 | 5521 | 3086 | 83 (7) |
| O(21) | −1630 (18) | 1720 (12) | 5544 (7) | 105 (8)* | C(65) | 4421 | 6436 | 3110 | 79 (7) |
| O(22) | −168 (20) | 105 (10) | 4038 (7) | 107 (8)* | C(66) | 3962 | 6823 | 2667 | 51 (5) |
| O(23) | −424 (26) | 2228 (15) | 2967 (6) | 142 (11)* | C(71) | 5420 (14) | 9064 (10) | 3154 (4) | 70 (6) |
| O(24) | −2787 (17) | 2682 (15) | 4305 (8) | 119 (9)* | C(72) | 6190 | 9686 | 3540 | 93 (8) |
| C(1) | 6386 (17) | 3526 (13) | 1325 (7) | 46 (7)* | C(73) | 5642 | 9960 | 3986 | 88 (7) |
| C(2) | 6931 (19) | 5429 (14) | 1188 (7) | 52 (7)* | C(74) | 4324 | 9612 | 4046 | 95 (8) |
| C(3) | 5797 (19) | 3970 (13) | 330 (7) | 50 (7)* | C(75) | 3554 | 8990 | 3660 | 82 (7) |
| C(4) | 7258 (18) | 1801 (13) | 721 (7) | 50 (7)* | C(76) | 4102 | 8716 | 3214 | 53 (5) |
| C(5) | 8292 (17) | 2575 (12) | −124 (6) | 43 (6)* | C(81) | 888 (17) | 6831 (10) | 2819 (6) | 105 (9) |
| C(6) | 10039 (21) | 1492 (13) | 488 (7) | 60 (8)* | C(82) | −520 | 6684 | 2846 | 120 (10) |
| C(7) | 12504 (19) | 2752 (13) | 808 (7) | 53 (7)* | C(83) | −1368 | 7473 | 2874 | 122 (10) |
| C(8) | 12642 (16) | 4756 (13) | 702 (6) | 44 (6)* | C(84) | −808 | 8409 | 2876 | 139 (12) |
| C(9) | 11583 (20) | 3283 (12) | −136 (7) | 59 (8)* | C(85) | 600 | 8556 | 2849 | 109 (9) |
| C(10) | 11671 (19) | 3525 (14) | 1761 (7) | 56 (7)* | C(86) | 1448 | 7767 | 2820 | 68 (6) |
| C(11) | 10451 (21) | 5323 (14) | 1513 (6) | 57 (8)* | | | | | |

[a] Asterisks denote equivalent isotropic $U$ values, defined as one-third of the trace of the orthogonalized $U_{ij}$ tensor.

those corresponding to Ru(1)–B(1) and Ru(3)–B(1), are equal in length within experimental error (2.111 (6) and 2.106 (6) Å).[33] In [5]⁻, the hydrogen-bridged edge is similar to the gold-bridged edge: Ru(1)–B(1) = 2.12 (2) Å compared to 2.10 (2) Å. This feature is consistent with the trend observed above for the auraferraboranes 1 and [4]⁻.

**Comparison of the Structures of [4]⁻ and [5]⁻.** Crystallographically characterized compounds in which a gold(I) center acts as a point of fusion for two cluster fragments and is four-coordinate are few.[6,34,35] A related silver(I) compound[36] and several mercury(II) species have been structurally characterized.[37–44] In several of these reports, the linking metal atom is described as being *sp*-hybridized and therefore pseudolinear as would be expected for Au(I), or Hg(II) species. The sp hybrid is involved in a three-center two-electron bridging interaction that renders the local environment about the heavy-metal atom four-coordinate. For the fusion of two simple triangular cluster units, there are two possible orientations (trans and cis) as shown in Figure 6a; these orientations are the extreme cases in which the gold and four "donor" atoms are taken as being coplanar. Recently, Di Vaira et

(34) Johnson, B. F. G.; Kaner, D. A.; Lewis, J.; Raithby, P. R. *J. Chem. Soc., Chem. Commun.* **1981**, 753.
(35) Di Vaira, M.; Stoppioni, P.; Peruzzini, M. *J. Chem. Soc., Dalton Trans.* **1990**, 109.
(36) Gade, L. H.; Johnson, B. F. G.; Lewis, J.; McPartlin, M.; Powell, H. R. *J. Chem. Soc., Chem. Commun.* **1990**, 110.
(37) Fajardo, M.; Gómez-Sal, M. P.; Holden, H. D.; Johnson, B. F. G.; Lewis, J.; McQueen, R. C. S.; Raithby, P. R. *J. Organomet. Chem.* **1984**, *267*, C25.
(38) Gómez-Sal, M. P.; Johnson, B. F. G.; Lewis, J.; Raithby, P. R.; Syed-Mustaffa, S. N. A. *J. Organomet. Chem.* **1984**, *272*, C21.
(39) Farrugia, L. J. *J. Chem. Soc., Chem. Commun.* **1987**, 147.
(40) Finster, D. C.; Grimes, R. N. *Inorg. Chem.* **1981**, *20*, 863.
(41) Johnson, B. F. G.; Kwik, W.-L.; Lewis, J.; Raithby, P. R.; Saharan, V. R. *J. Chem. Soc., Dalton Trans.* **1991**, 1037.
(42) Gong, J.; Huang, J.; Fanwick, P. E.; Kubiak, C. P. *Angew. Chem., Int. Ed. Engl.* **1990**, *29*, 396.
(43) Ermer, S.; King, K.; Hardcastle, K. I.; Rosenberg, E.; Manotti Lanfredi, A. M.; Tiripicchio, A.; Tiripicchio Camellini, M. *Inorg. Chem.* **1983**, *22*, 1339.
(44) Rosenberg, E.; Hardcastle, K. I.; Day, M. W.; Gobetto, R.; Hajela, S.; Muftikian, R. *Organometallics* **1991**, *10*, 203.

**Table VIII. Selected Bond Distances (Å) and Angles (deg) for One of the Crystallographically Independent Half Anions $[5]^-$**

| molecule A | | molecule B | |
|---|---|---|---|
| | (a) Bond Distances | | |
| Ru(1)–Ru(2) | 2.834 (2) | Ru(7)–Ru(8) | 2.827 (2) |
| Ru(1)–Ru(4) | 2.823 (2) | Ru(6)–Ru(7) | 2.823 (2) |
| Ru(2)–Ru(3) | 2.851 (2) | Ru(5)–Ru(6) | 2.860 (2) |
| Ru(2)–Ru(4) | 2.878 (2) | Ru(6)–Ru(8) | 2.893 (2) |
| Ru(3)–Ru(4) | 2.858 (2) | Ru(5)–Ru(8) | 2.865 (2) |
| Ru(1)–B(1) | 2.123 (24) | Ru(7)–B(2) | 2.175 (20) |
| Ru(2)–B(1) | 2.197 (18) | Ru(6)–B(2) | 2.205 (22) |
| Ru(3)–B(1) | 2.099 (24) | Ru(5)–B(2) | 2.053 (20) |
| Ru(4)–B(1) | 2.200 (20) | Ru(8)–B(2) | 2.215 (17) |
| Ru(3)–Au(1) | 2.700 (1) | Ru(5)–Au(2) | 2.711 (1) |
| Au(1)–Ru(3A) | 2.700 (1) | Au(2)–Ru(5A) | 2.711 (1) |
| Au(1)–B(1) | 2.322 (21) | Au(2)–B(2) | 2.288 (19) |
| Au(1)–B(1A) | 2.323 (21) | Au(2)–B(2A) | 2.288 (19) |
| | (b) Bond Angles | | |
| Ru(2)–Ru(1)–Ru(4) | 61.2 (1) | Ru(6)–Ru(7)–Ru(8) | 61.6 (1) |
| Ru(2)–Ru(1)–B(1) | 50.1 (5) | Ru(6)–Ru(7)–B(2) | 50.3 (6) |
| Ru(4)–Ru(1)–B(1) | 50.4 (5) | Ru(8)–Ru(7)–B(2) | 50.5 (5) |
| Ru(1)–Ru(2)–RU93) | 94.0 (1) | Ru(7)–Ru(6)–Ru(5) | 94.1 (1) |
| Ru(1)–Ru(2)–Ru(4) | 59.2 (1) | Ru(7)–Ru(6)–Ru(8) | 59.3 (1) |
| Ru(3)–Ru(2)–Ru(4) | 59.8 (1) | Ru(5)–Ru(6)–Ru(8) | 59.7 (1) |
| Ru(1)–Ru(2)–B(1) | 47.9 (6) | Ru(7)–Ru(6)–B(2) | 49.4 (5) |
| Ru(3)–Ru(2)–B(1) | 47.0 (6) | Ru(5)–Ru(6)–B(2) | 45.6 (5) |
| Ru(4)–Ru(2)–B(1) | 49.2 (5) | Ru(8)–Ru(6)–B(2) | 49.3 (5) |
| Ru(2)–Ru(3)–Ru(4) | 60.5 (1) | Ru(6)–Ru(5)–Ru(8) | 60.7 (1) |
| Ru(2)–Ru(3)–Au(1) | 94.3 (1) | Ru(6)–Ru(5)–Au(2) | 95.0 (1) |
| Ru(4)–Ru(3)–Au(1) | 99.2 (1) | Ru(8)–Ru(5)–Au(2) | 97.8 (1) |
| Ru(2)–Ru(3)–B(1) | 49.9 (5) | Ru(6)–Ru(5)–B(2) | 50.1 (6) |
| Ru(4)–Ru(3)–B(1) | 49.9 (5) | 4u(8)–Ru(5)–B(2) | 50.3 (5) |
| Au(1)–Ru(3)–B(1) | 56.2 (6) | Au(2)–Ru(5)–B(2) | 55.3 (5) |
| Ru(1)–Ru(4)–Ru(2) | 59.6 (1) | Ru(7)–Ru(8)–Ru(6) | 59.1 (1) |
| Ru(1)–Ru(4)–Ru(3) | 94.1 (1) | Ru(7)–Ru(8)–Ru(5) | 93.9 (1) |
| Ru(2)–Ru(4)–Ru(3) | 59.6 (1) | Ru(6)–Ru(8)–Ru(5) | 59.6 (1) |
| Ru(1)–Ru(4)–B(1) | 48.1 (6) | Ru(7)–Ru(8)–B(2) | 49.3 (5) |
| Ru(2)–Ru(4)–B(1) | 49.1 (5) | Ru(6)–Ru(8)–B(2) | 49.0 (6) |
| Ru(3)–Ru(4)–B(1) | 46.8 (6) | Ru(5)–Ru(8)–B(2) | 45.5 (5) |
| Ru(1)–B(1)–Ru(3) | 160.1 (11) | Ru(7)–B(2)–Ru(5) | 159.4 (11) |
| Ru(1)–B(1)–Ru(4) | 81.5 (8) | Ru(7)–B(2)–Ru(8) | 80.2 (6) |
| Ru(3)–B(1)–Ru(4) | 83.3 (8) | Ru(5)–B(2)–Ru(8) | 84.2 (7) |
| Ru(1)–B(1)–Ru(2) | 82.0 (8) | Ru(7)–B(2)–Ru(6) | 80.2 (7) |
| Ru(2)–B(1)–Ru(3) | 83.1 (7) | Ru(6)–B(2)–Ru(5) | 84.3 (8) |
| Ru(2)–B(1)–Ru(4) | 81.8 (7) | Ru(6)–B(2)–Ru(8) | 81.8 (7) |
| Ru(1)–B(1)–Au(1) | 124.7 (10) | Ru(7)–B(2)–Au(2) | 123.5 (9) |
| Ru(3)–B(1)–Au(1) | 75.1 (7) | Ru(5)–B(2)–Au(2) | 77.1 (6) |
| Ru(3)–Au(1)–B(1) | 48.7 (6) | Ru(5)–Au(2)–B(2) | 47.6 (5) |
| Ru(3A)–Au(1)–B(1) | 131.3 (6) | Ru(5A)–Au(2)–B(2) | 132.4 (5) |
| B(1)–Au(1)–B(1A) | 180.0 (1) | B(2)–Au(2)–B(2A) | 180.0 (1) |

al., have shown that, in solution, the gold atom that fuses together two $P_3$ units in $[\{MeC(CH_2PPh_2)_3\}MP_3\}_2Au]^+$ (M = Co, Rh, Ir) is fluxional with respect to motion over the $P_3$ fragments, thereby rendering all six phosphorus atoms equivalent; this effectively equilibrates the trans and cis isomers, although the trans isomer is preferred in the solid state.[35]

The fusion of two cluster units, each of which possesses two different "donor sites" (as in the metallaboranes reported here), leads to the possibility of cis and trans isomers with respect to a formal square-planar coordination sphere (Figure 6b). The sp hybrid bonding scheme naturally allows flexibility with respect to the orientation of the two cluster subunits, and limiting coordination geometries will be square planar ($\alpha$ = 0 or 180°) and tetrahedral ($\alpha$ = 90°). The work of Rosenberg et al. has indicated that, at temperatures above −40 °C, the triruthenium-based cluster subunits in $\{Ru_3(CO)_9(C_2{}^tBu)\}_2Hg$ undergo motion with respect to the central mercury atom such that there is rapid interconversion of the cis and trans isomers.[45] In Table IX, values of $\alpha$ (defined in the table) are listed for structurally characterized members of this growing group of compounds. It would appear, both in summarizing

(45) Hajela, S.; Novak, B. M.; Rosenberg, E. *Organometallics* **1989**, *8*, 468.

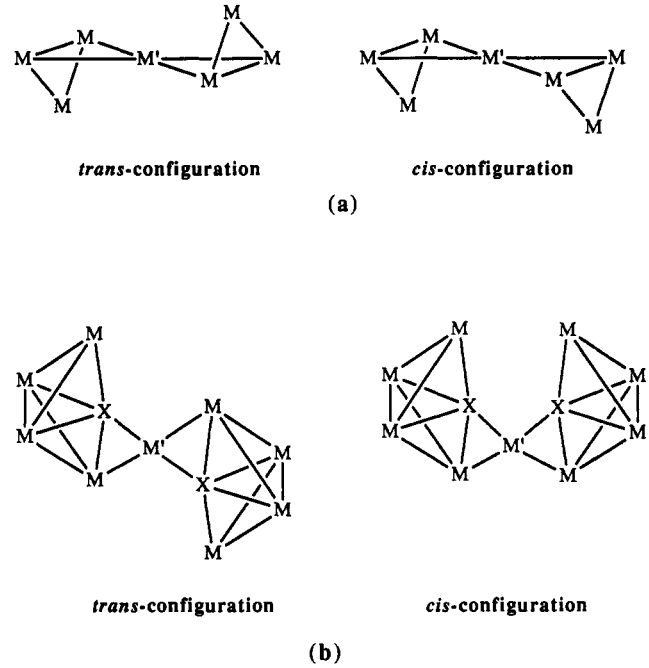


**Figure 6.** Possible geometries for the fusion of two cluster subunits: (a) two $M_3$ units bonded to the central atom (M′) via M–M′–M bridges mutually trans or cis with respect to the orientations of the $M_3$ units; (b) two $M_4X$ asymmetrical subunits bonded via M–(M′)–X interactions mutually trans or cis with respect to the placement of the M and X atoms.

**Table IX. Comparison of the Geometries at the Four-Coordinate Central Atom Ag(I), Au(I), or Hg(II) in Fused Compounds of the Type $[\{cluster\}_2M]^{n\pm}$ [a]**

| compd | angle $\alpha$ (deg) | ref |
|---|---|---|
| $[\{HOs_3(CO)_{10}\}_2Au]^-$ | 0[b] | 34 |
| $[\{HOs_3(CO)_{10}\}_2Ag]^-$ | 0[b] | 36 |
| $\{CpCoB_3H_4C_2Me_2\}_2Hg$ | 0[b] | 40 |
| $\{Ru_3(CO)_{10}(\mu\text{-}NO)\}_2Hg$ | 27.6 | 38 |
| $[\{HFe_4(CO)_{12}BH\}_2Au]^-$ | 30.9 (5) | 6, this work |
| $[\{Ni_2(\mu\text{-}CNMe)(CNMe)_4(dppm)\}_2Hg]^{2+}$ | 34.6 (1) | 42 |
| $[\{Os_{10}(CO)_{24}C\}_2Hg]^{2-}$ | 38.4 | 36 |
| $\{Ru_3(CO)_9(C_2{}^tBu)\}_2Hg$ | 44.6 | 43 |
| $\{CpCoFe_2(CO)_7(\mu_3\text{-}COMe)\}_2Hg$ | 46.2 | 39 |
| $[\{(MeC(CH_2PPh_2)_3)CoP_3\}_2Au]^+$ | 50.4 (3) | 35 |
| $[\{(MeC(CH_2PPh_2)_3)RhP_3\}_2Au]^+$ | 51.1 (1) | 35 |
| $[\{(MeC(CH_2PPh_2)_3)IrP_3\}_2Au]^+$ | 51.5 (4) | 35 |
| $\{H(\mu_3\text{-}S)Os_3(CO)_9\}_2Hg$ | 65 | 44 |
| $\{CpRhFe_2(CO)_7(\mu_3\text{-}COMe)\}_2Hg$ | 71.9 | 39 |
| $[\{Ru_6(CO)_{16}C\}_2Hg]^{2-}$ | 74[c] | 41 |
| $[\{HRu_4(CO)_{12}BH\}_2Au]^-$ | 180[d] | this work |

[a] $\alpha$ is defined as 0 or 180° for a square-planar geometry and 90° for tetrahedral coordination. [b] Trans isomer as defined in Figure 6a. [c] Value calculated by us from atomic coordinates. [d] Trans isomer as defined in Figure 6b.

comments made by individual authors[39,40,42] and by inspection of the structures themselves, that the values of $\alpha$ obtained for the solid state are determined primarily by a combination of intramolecular steric and crystal-packing effects.

Anions $[4]^-$ and $[5]^-$ represent an interesting pair of compounds that differ only by a change from first- to second-row transition metal in the cluster subunit. The $\{Ru_4(CO)_{12}\}$ fragment is larger than its iron counterpart, and bond lengths involving the gold atom in $[4]^-$ (Figure 3) are Fe(4)–Au(1) = 2.615 (1) Å and Au(1)–B = 2.300 (12) Å and in $[5]^-$ (Figure 5) are Ru(3)–Au(1) = 2.700 (1) Å and Au(1)–B(1) = 2.32 (2) Å. This increase in skeletal size does not necessarily permit a greater separation between carbonyl ligands attached to adjacent cluster subunits, since

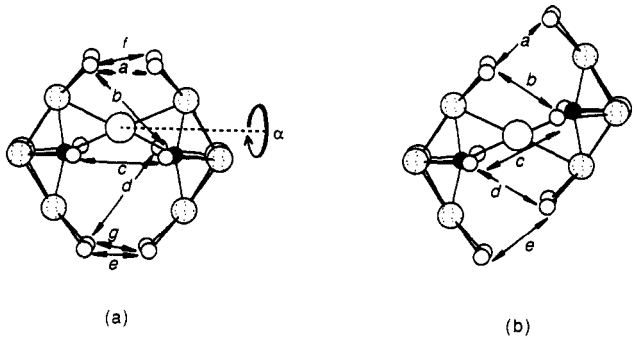


**Figure 7.** Labeling scheme for nonbonded carbonyl separations in model trans and cis isomers of $[\{HM_4(CO)_{12}BH\}_2Au]^-$ (M = Fe, Ru): (a) $\alpha = 0°$; (b) $\alpha = 180°$. In each model, the gold atom is in a planar environment. Carbonyl ligands not involved in close contacts are omitted for clarity.

there is a significant increase in the average M–CO distance from iron (average 1.794 Å in $[4]^-$) to ruthenium (average 1.920 Å in $[5]^-$). Those nonbonded separations that will be important in determining minimal energy conformations for the two anions are shown in Figure 7.[46] The two extreme arrangements (viz. cis and trans isomers with a planar environment at the gold atom) have values of $\alpha = 0$ and 180°, respectively. For $\alpha = 0°$ and M = Fe, the shortest nonbonded CO···OC separation is 2.5 Å,[46] while for M = Ru, it is 2.3 Å.[46] For $\alpha = 180°$ and M = Fe, Ru, the shortest CO···OC distance is 3.2 and 3.1 Å, respectively.[46] Noting that the sum of the van der Waals radii of two oxygen atoms is 3.0 Å,[47] we suggest that, as a result of steric factors, the trans isomer should be favored over the cis for *both* M = Fe and M = Ru. However, the crystallographic data confirm this structure only for M = Ru.

In an attempt to understand the structural preference shown by anion $[4]^-$, we have followed changes in the nonbonded carbonyl separations as a function of angle $\alpha$ starting from a model compound with the unfavorable cis isomer ($\alpha = 0°$) for M = Fe. Repulsive interactions such as those labeled *a*, *c*, and *e* in Figure 7 are "turned off" as $\alpha$ increases, but at the same time, new and significant cross-interactions (*f* and *g* in Figure 7a) are "turned on". The experimental angle in $[4]^-$ of $\alpha = 30.9°$ corresponds to a relatively favorable balance between these two sets of interactions. A value of $\alpha$ in the range of ~40–65° leads to exceptionally short CO···OC separations for *f* and *g*. We suggest that the crystallographically determined structure for anion $[5]^-$ is as would be predicted by steric considerations but that the observed structure of $[4]^-$ (Figure 3) is a result of a combination of steric effects and crystal-packing effects. Perhaps it is significant that the cation is not common to the crystallographically determined structures reported here, but on the other hand, there are no apparent cation–anion interactions in either structure.

**Relationship between $[4]^-$ or $[5]^-$ and 1 or 2.** The formation of either of the cluster anions $[4]^-$ and $[5]^-$ must proceed via Au–P bond cleavage, and it seems reasonable to propose that these anions are generated respectively via the monogold derivatives **1** and **2**. This is most easily understood if we consider the formation of $[AuL_2][4]$ (L = $P(2\text{-Me-}C_6H_4)_3$, $PMe_3$, $PEt_3$, $PMe_2Ph$, $PMePh_2$), in which the stoichiometry of the compound is identical with that of the monogold derivative $HFe_4(CO)_{12}BHAuL$. The

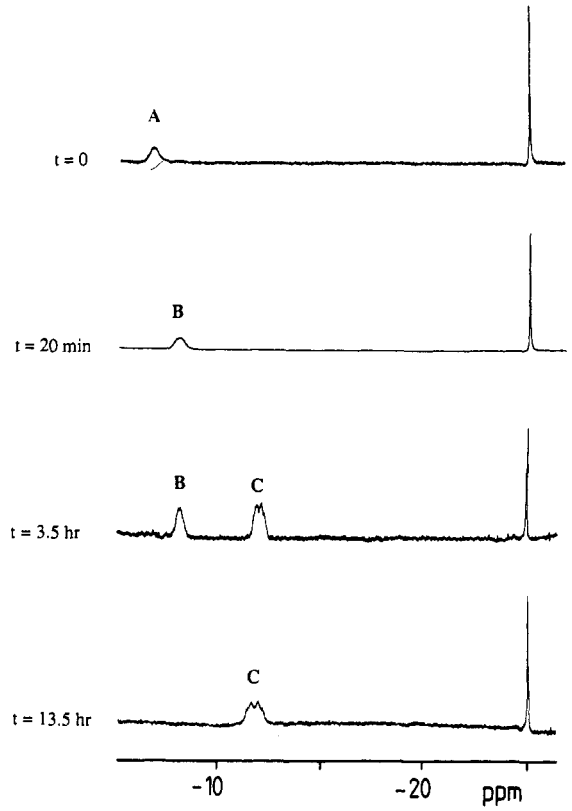


**Figure 8.** Reaction of $[Au\{P(2\text{-Me-}C_6H_4)_3\}_2][4]$ with concentrated HCl monitored over a period of 13.5 h by $^1H$ NMR spectroscopy. Resonances corresponding to Fe–H–B bridging protons in $[4]^-$, **1**, and $HFe_4(CO)_{12}BH_2$ are labeled A–C, respectively. Signals for the Fe–H–Fe protons are coincident for the three compounds.

relationship between $[AuL_2][4]$ and $HFe_4(CO)_{12}BHAuL$ may be described in terms of a ligand redistribution (eq 2).

$$2HFe_4(CO)_{12}BHAuL \rightarrow [AuL_2]^+ + [\{HFe_4(CO)_{12}BH\}_2Au]^- \quad (2)$$

In order to test the role of **1** as a direct precursor to $[AuL_2][4]$, a sample of pure **1** was combined in dichloromethane with molar equivalents of both $[PPN][HFe_4(CO)_{12}BH]$ and $(2\text{-Me-}C_6H_4)_3PAuCl$ in the presence of $TlPF_6$. Within 10 min, the solution had changed from brown to dark green and, after chromatographic separation, $[Au\{P(2\text{-Me-}C_6H_4)_3\}_2][4]$ was isolated in ~50% yield. One related cluster fusion reaction that has previously been reported is the formation of $[PPN][\{HOs_3(CO)_{10}\}_2Au]$. Significantly, this compound is generated by treating the monogold derivative $HOs_3(CO)_{10}AuPR_3$ (R = Et, Ph) with [PPN]Cl.[32] However, when **1** was treated with [PPN]Cl, the only recoverable products were $[PPN][HFe_4(CO)_{12}BH]$ and $(2\text{-Me-}C_6H_4)_3PAuCl$.

The process of cluster fusion may be reversed by combining $[Au\{P(2\text{-Me-}C_6H_4)_3\}_2][4]$ with either [PPN]Cl or acid. Reaction with [PPN]Cl in dichloromethane solution at room temperature resulted in the formation of $[PPN][HFe_4(CO)_{12}BH]$ within 15 min, and no intermediate compound was detected. However, the addition of concentrated hydrochloric acid to $[Au\{P(2\text{-Me-}C_6H_4)_3\}_2][4]$ in $CH_2Cl_2$ resulted in a slow reaction that could be monitored by infrared or $^{11}B$ or $^1H$ NMR spectroscopy. Over a period of 13 h, the decay of $[Au\{P(2\text{-Me-}C_6H_4)_3\}_2][4]$ was observed to give first **1** and then $HFe_4(CO)_{12}BH_2$ (Figure 8). Changes in the region of the spectrum associated with the Fe–H–B bridging hydrogen atom proved to be the most instructive method of monitoring the transformations, with

(46) Calculated distances are only approximate and clearly reflect the molecular symmetry inherent in each of the structures depicted in Figures 3 and 5.

(47) Bondi, A. *J. Phys. Chem.* **1964**, *68*, 441.

the respective $^1H$ NMR resonance shifting from $\delta$ −6.4 for [4]$^-$ to $\delta$ −7.7 for 1 and finally to $\delta$ −11.9 for $HFe_4(CO)_{12}BH_2$[22] (treatment of pure 1 with concentrated HCl generates $HFe_4(CO)_{12}BH_2$ and (2-Me-$C_6H_4)_3$PAuCl more or less quantitatively). [Au{P(2-Me-$C_6H_4)_3$}$_2$][4] is rapidly and cleanly converted to 1, while complete regeneration of the all-hydrogenated butterfly cluster is a much slower process. There was no attempt to make a detailed kinetic study of the degradation mechanism.

### To Fuse or Not to Fuse?

The reaction of $[HFe_4(CO)_{12}BH]^-$ with 1 equiv of LAuCl leads to the simple monogold derivative $HFe_4(CO)_{12}BH$-AuL, which is stable with respect to conversion to $HFe_4(CO)_{12}BAu_2L_2$ only when L is the sterically demanding ligand P(2-Me-$C_6H_4)_3$. In other cases (L = $PMe_3$, $PEt_3$, $PMe_2Ph$, $PMePh_2$) the preferred product is $[AuL_2][\{HFe_4(CO)_{12}BH\}_2Au]$, which, although possessing the same stoichiometry as $HFe_4(CO)_{12}BHAuL$, contains two $\{HFe_4(CO)_{12}BH\}$ subclusters fused about a gold(I) atom and results from Au–P cleavage and a redistribution of the phosphine ligands. As one goes from $[HFe_4(CO)_{12}BH]^-$ to the ruthenium analog, the tetrametal butterfly increases in size and the reaction of $[HRu_4(CO)_{12}BH]^-$ with LAuCl, even in the case of L = P(2-Me-$C_6H_4)_3$, leads to the competitive formation of $HRu_4(CO)_{12}BHAuP$(2-Me-$C_6H_4)_3$ and $Ru_4(CO)_{12}BHAu_2${P(2-Me-$C_6H_4)_3$}$_2$ as well as $[\{HRu_4(CO)_{12}BH\}_2Au]^-$. For the ruthenium clusters, the fused system $[\{HRu_4(CO)_{12}BH\}_2Au]^-$ appears to be a particularly favorable product.

**Acknowledgments** are made to the donors of the Petroleum Research Fund, administered by the American Chemical Society, for support of this work, to the SERC for a studentship (to S.M.D.), to the Cambridge Commonwealth Trust and Tate and Lyle Corp. for a studentship (to M.S.S.), and to the NSF for a grant (CHE 9007852) toward the purchase of a diffractometer at the University of Delaware. Johnson-Matthey is thanked for generous loans of $RuCl_3$. C.E.H. thanks Dr. Lutz H. Gade for several useful discussions.

**Registry No.** 1, 141292-25-3; 2, 141292-27-5; 3 (isomer 1), 141292-34-4; 3 (isomer 2), 141319-39-3; 4, 141292-33-3; [PPN][4], 141292-32-2; [PPN][5], 141292-36-6; [Au{P(2-Me-$C_6H_4)_3$}$_2$][5], 141292-31-1; 6, 141292-28-6; $[Et_3NH][Fe_4(CO)_{12}BHAuP$(2-Me-$C_6H_4)_3$}], 141319-38-2; $HFe_4(CO)_{12}BHAu$P(c-$C_6H_{11})_3$}, 141292-26-4; $[Et_3NH][HRu_4(CO)_{12}BAuP$(2-Me-$C_6H_4)_3$}], 141319-36-0; [PPN][$HFe_4(CO)_{12}BH$], 108008-77-1; {(2-Me-$C_6H_4)_3$}PAuCl, 83076-07-7; {(c-$C_6H_{11})_3$}PAuCl, 49763-41-9; ClAu(dppm)AuCl, 37095-27-5; Au, 7440-57-5; Fe, 7439-89-6; $Ru_4(CO)_{12}BAu_3${P(2-Me-$C_6H_4)_3$}$_3$, 141292-29-7; Ru, 7440-18-8; [PPN][$HRu_4(CO)_{12}BH$], 125476-27-9.

**Supplementary Material Available:** Tables of bond distances, bond angles, thermal parameters, and H atom coordinates for 1, [Au($PMePh_2$)$_2$][4], and [PPN][5] (17 pages). Ordering information is given on any current masthead page.

OM9107707

# Gas-Phase Reactions of Molybdenum Oxide Ions with Small Hydrocarbons

Carolyn J. Cassady*

*Department of Chemistry, Miami University, Oxford, Ohio 45056*

Stephen W. McElvany

*Code 6113/Chemistry Division, Naval Research Laboratory, Washington, D.C. 20375-5000*

*Received October 25, 1991*

The gas-phase ion/molecule reactions of $Mo^+$, $MoO^+$, and $MoO_2^+$ with small alkanes, alkenes, and $C_6$ hydrocarbons have been investigated using Fourier transform ion cyclotron resonance mass spectrometry. Product branching ratios and reaction rate constants are reported. Dehydrogenation dominates the reactions, with little cleavage of the strong $Mo^+$–O and $OMo^+$–O bonds. Aside from the production of $MoO(CO)^+$ from $MoO_2^+$ and ethene, no evidence is found for the formation of oxygenated hydrocarbons, either as neutral reaction products or as ligands bound to $Mo^+$. However, the reactions of $Mo^+$, $MoO^+$, and $MoO_2^+$ differ in terms of both rates and pathways. In contrast to the slow reaction rates of the $d^5$ system $Mo^+$, several $MoO^+$ and $MoO_2^+$ reactions proceed at or near the collision rate. Variations are also seen in product ion distributions, and for $MoO_2^+$, unique reaction pathways involving dehydration and the elimination of small hydrocarbons occur. While $Mo^+$ and $MoO^+$ yield only products which are the result of C–H insertion, $MoO_2^+$ is capable of inserting into the C–C bonds of organic molecules.

## Introduction

Transition-metal oxides are common catalysts in oxidation processes. Oxygen atom transfer involving oxometal groups (M=O) plays a prominent role in these reactions. Although many transition-metal compounds can undergo oxygen transfer, molybdenum compounds are the most widely studied and employed. Over 100 oxygen-transfer reactions have been characterized for molybdenum compounds.[1] These involve a wide range of processes, including the epoxidation of alkenes[2] and alcohols,[3] the ammoxidation of alkenes to nitriles,[4] the oxyhydration of alkenes to alcohols, aldehydes, and ketones,[5] the oxidative

(1) (a) Holm, R. H. *Chem. Rev.* **1987**, *87*, 1401. (b) Kung, H. H. *Transition Metal Oxides: Surface Chemistry and Catalysis*; Studies in Surface Science and Catalysis Series; Elsevier: New York, 1989; Vol. 45.

(2) (a) Landau, R.; Sullivan, G. A.; Brown, D. *Chemtech* **1979**, *9*, 602. (b) Mimoun, H.; Seree de Roch, I.; Sajus, L. *Tetrahedron* **1970**, *26*, 37. (c) Chong, A. O.; Sharpless, K. B. *J. Org. Chem.* **1977**, *42*, 1587. (d) Daniel, C.; Keulks, G. W. *J. Catal.* **1972**, *24*, 529.

(3) Sharpless, K. B.; Verhoeven, T. R. *Aldrichim. Acta* **1979**, *12*, 63.

(4) (a) Reddy, B. M.; Narsimha, K.; Sivaraj, C.; Roa, P. K. *Appl. Catal.* **1989**, *55*, L1. (b) Burrington, J. D.; Kartisch, C. T.; Grasselli, R. K. *J. Catal.* **1983**, *81*, 489. (c) Burrington, J. D.; Kartisch, C. T.; Grasselli, R. K. *J. Catal.* **1984**, *87*, 363.

(5) (a) Tan, S.; Moro-oka, Y.; Ozaki, A. *J. Catal.* **1970**, *17*, 125. (b) Moro-oka, Y.; Takita, Y.; Ozaki, A. *J. Catal.* **1971**, *23*, 183. (c) Pitchai, R.; Klier, K. *Catal. Rev.* **1986**, *28*, 13. (d) Khan, M. M.; Somorjai, G. A. *J. Catal.* **1986**, *28*, 13.

0276-7333/92/2311-2367$03.00/0 